ABSTRACT

Title of Thesis: A STUDY OF PLANAR AND NONPLANAR MEMBRANE WING PLANFORMS FOR THE DESIGN OF A FLAPPING-WING MICRO AIR VEHICLE

Beverly Beasley, Masters of Science, 2006

Thesis Directed by: Prof. Inderjit Chopra
Department of Aerospace Engineering

Flapping wings may have potential for success in the realm of micro air vehicles (MAVs). The goal of this thesis was to investigate a variety of flapping wing planforms, including nonplanar effects, to create an optimum planform for an MAV design. Test stand and model prototype experiments were conducted to measure the lift and propulsive thrust generated by flapping wing planforms with a variety of nonplanar tips. The polynomial planform with 20º tip anhedral was selected for the flapping-wing MAV designed herein because of its enhanced performance, reaching over 15 g of lift. A propulsive thrust analysis was performed on the selected wing, indicating sufficient levels of thrust production. Instantaneous lift and strobe photography analyses were performed to investigate the underlying physical effects of nonplanar tips, particularly their ability to reduce negative upstroke lift.

A STUDY OF PLANAR AND NONPLANAR MEMBRANE WING PLANFORMS FOR THE DESIGN OF A FLAPPING-WING MICRO AIR VEHICLE

by

Beverly Beasley

Thesis submitted to the faculty of the Graduate School of the
University of Maryland, College Park in partial fulfillment
of the requirements for the degree of
Masters of Science
2006

Advisory Committee:

Professor Inderjit Chopra, Chair/Advisor
Professor Norman Wereley
Professor James Baeder

This dissertation is dedicated to my Mother and Father.

ACKNOWLEDGEMENTS

I would like to thank the National Science Foundation for supporting this work under a Graduate Research Fellowship. I would also like to extend my gratitude to the following people for their contributions to this research: to Dr. Chopra for being my graduate advisor, Beerinder Singh for teaching me so many things in the lab and providing guidance and advice for my research, Felipe Bohorquez for helping with preparations for the wind tunnel tests, Lynn Gravatt for her assistance with LabVIEW setup (and the smoke generator fiasco), Anubhav Datta for his excellent proofreading skills, Moble Benedict and Peter Copp for assisting with powered-glide tests, and especially to my fiancé, Tim Miller, for his unconditional support in so many ways.

TABLE OF CONTENTS

LIST OF TABLES

LIST OF FIGURES

Nomenclature

α_f = fuselage angle of attack
μ = dynamic viscosity
ρ = density
AR = aspect ratio
b = total wing span
C_L = lift coefficient
C_T = propulsive thrust coefficient
f = flapping frequency
l = characteristic length
L = lift
L/D = lift-to-drag ratio
M = mass
Re = Reynolds number
S = wing planform area
T = propulsive thrust
V = freestream velocity

Chapter

1 Introduction

The growing interest in unmanned aircraft, especially for surveillance in constrained areas, has triggered much research in the area of micro air vehicles (MAVs). Sensors and actuators are becoming smaller and smarter, enabling new aircraft designs. MAVs offer the potential to fly reconnaissance missions in constrained areas, which are difficult for larger aircraft to accomplish. Their small size allows them to navigate in tight corners at low speeds and blend in with their surroundings. The opportunity exists to build low cost systems that can hover or take off in short distances, generate less noise, and be quickly deployed in the field.

1.1 What are Micro Air Vehicles?

In 1997, the Defense Advanced Research Projects Agency (DARPA) initiated a program to develop and test MAVs for military surveillance and reconnaissance missions. DARPA defined the MAV in terms of size, gross weight, and payload—requiring that the maximum dimension in any direction be no greater than 15 cm, the gross weight should not exceed 100 g, with up to 20 g devoted to payload, and the MAV should be able to reach altitudes of up to 100 m [1]. These requirements directed research toward emerging technologies that would enable the flight of small vehicles. As a result, many institutions began investigating various MAV concepts. These MAVs took the form of fixed-wing, rotary-wing, and flapping-wing configurations, among others. Most operated below chord-based Reynolds numbers of 100,000, where conventional aerodynamic theories are inadequate. The Reynolds number is a ratio of inertial to viscous aerodynamic forces used to characterize flight regimes, and is defined in Equation 1.1.

$$\mathrm{Re} = \frac{Inertial}{Viscous} = \frac{\rho S V^2}{\mu S V / l} = \frac{\rho l V}{\mu} \tag{1.1}$$

where ρ is the fluid density, l is a characteristic length (in this case, the chord), V is the fluid velocity, and μ is the dynamic viscosity of the fluid [2]. Figure 1.1 illustrates the Reynolds number flight regime where MAVs operate as compared to other manned and unmanned aircraft.

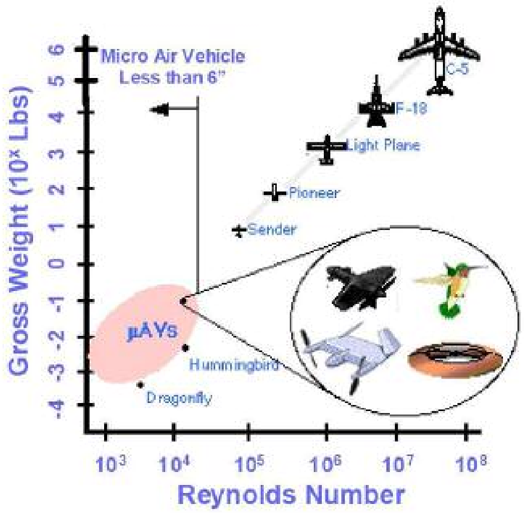

Figure 1.1: MAV Flight Regime [1]

DARPA's current MAV initiative is the Advanced Concept Technology Demonstration phase [3], which seeks to further develop practical MAV systems for military use. Whereas the initial phase focused on individual components in MAV flight, the current phase focuses on technologies that will allow MAVs to accomplish missions in restricted environments with autonomous or semi-autonomous control. These technologies focus more on navigation, communications, and multi-task subsystems, particularly because MAV missions could require navigation inside buildings, in densely populated areas, or in mountainous terrain, caves, or heavily forested areas. Other MAV missions might include sensor dispersal, border surveillance, electronic jamming, communications, counter-drug operations, mine detection, and biological and chemical agent detection.

DARPA’s initiatives uncovered limitations in aerodynamics, flight controls, propulsion, navigation, communication, and multi-function subsystems for small scale systems. Thus, many MAV concepts developed suffered from limited range and endurance [3]. The limitations mentioned above are dicussed below.

1.1.1 Aerodynamics

As shown in Figure 1.1, the small length and low velocities of MAVs result in a very low Reynolds number flight regime. At this scale, the aerodynamic regime is referred to as a laminar region where viscous forces dominate the airflow, and conventional steady aerodynamic theories based on turbulent flow regimes are no longer valid. For this reason, conventional fixed-wing airfoils suffer from severe performance degradation at low Reynolds numbers. Hence, phenomena associated with generation of steady and unsteady aerodynamic forces need reevaluation in this flight regime. While much empiricism has been used to study bird and insect flight in this complex regime, our understanding of the aerodynamics involved is still limited. Investigations and observations from nature appear to indicate that wing flexibility and flapping are two specific mechanisms that can overcome many limitations associated with low Reynolds number regime limitations, as exemplified in birds and insects. However, mimicking avian or insect aeromechanics precisely is difficult for a number of reasons.

Birds and insects do not fly by means of a simple up and down flapping motion of the wings, instead they use several subtle mechanisms that modify the vertical flapping motion. In forward flight, the wing stroke is tilted about 30º from the vertical (though the exact angle varies with flight speed and among flying animals and insects), such that the wings move slightly forward on the downstroke, and slightly back on the upstroke relative to the body. The wingtip stroke patterns relative to the body indicate further complexity, as illustrated in Figure 1.2 [4].

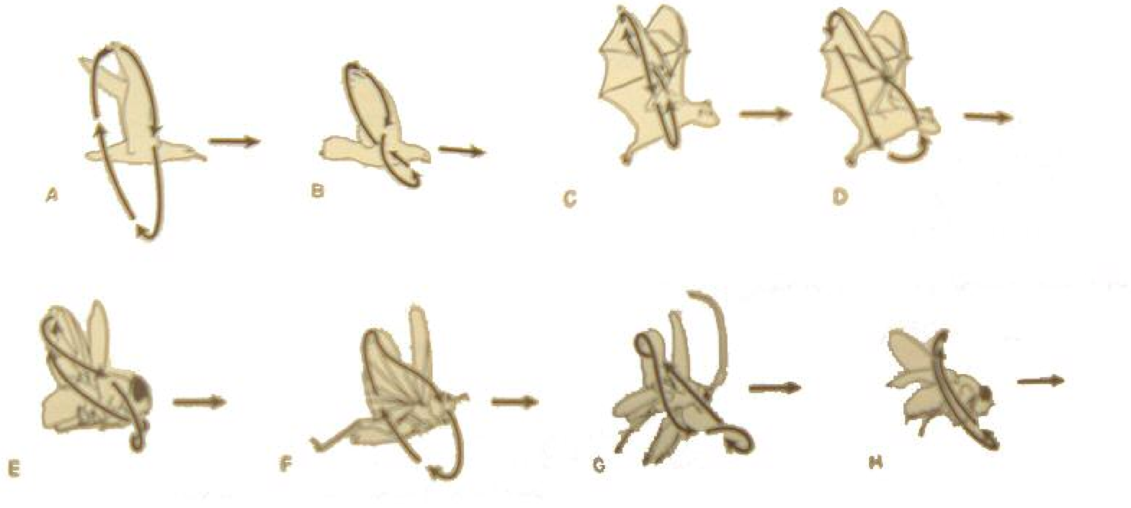

Figure 1.2: Wingtip Paths of Various Flyers (A. Albatross, B. Pigeon, C. Horseshoe Bat in Fast Flight, D. Horseshoe Bat in Slow Flight, E. Blow Fly, F. Locust, G. June Beetle, H. Fruit Fly) [4]

The wingtip strokes of larger birds follow simple patterns like ovals or figure-eights for albatrosses and pigeons, respectively. As the size of the animal decreases, the wingtip pattern becomes increasingly complicated. For example, june beetles' and blowflies' wingtip patterns include several complex loops. By looking at the wingtip patterns relative to the air, we see a similar correlation as size of the animal decreases. The wingtips of large birds will follow a pattern that is nearly sinusoidal, whereas the wingtips of smaller birds and insects have upstrokes which become more vertical or in some cases are angled away from the direction of flight. As the size of the animal decreases, the flapping frequency increases and the upstroke increasingly tends to have a shorter duration than the downstroke. Additionally, birds and insects actively change the angle of attack of their wings during the downstroke and upstroke. Birds also reduce the surface area of their wings during the upstroke, either by turning their feathers or folding their wings to reduce drag. These differences between the upstroke and downstroke largely account for a bird or insect's ability to sustain flight [4].

The physical mechanisms of bird and insect flight are not the only means by which they are able to fly. Birds and insects are able to harness the use of bound and trailing vortices, which are unsteady effects. Vortices are concentrated areas of circulation, which create large suction forces that account for some proportion of lift produced on many birds and insects. Large birds that travel at fast forward speeds create a wake that consists of a pair of continuous undulating vortex streams behind the wingtips, these vortices do not contribute lift directly, but are rather a result of the lift generated by the wings alone. Small songbirds and bats create a bound vortex sheet on the downstroke that produces lift, then they shed the bound vortex on the upstroke, resulting in a stack of circular vortex rings in the animal's wake. As the size of birds and insects decrease, the animal must work harder to produce vortices because of the increasingly viscous flow regime. Some insects change the angle of attack of their wings in such a way that the bound vortex created on the downstroke stays attached during the upstroke, providing a constant source of vortex lift. Other insects produce bound vortices between their wings by clapping their wings together at the top of the upstroke, as the wings are pulled apart, a vortex forms—known as the clap-fling mechanism. Some bats and birds use the clap-fling mechanism to momentarily produce the large required lift necessary for takeoff and landing [4].

All of these naturally-occurring movements and lift mechanisms are difficult to replicate in MAVs. The complex motions of natural flight are difficult to replicate mechanically without adding a large amount of weight to the MAV. Birds and insects are able to subtlety change the motion of their wings to respond to wind gusts and changing flight modes, which would translate into the need for a sophisticated feedback control system on an MAV. Overall, it is difficult to mimick natural flight precisely because of the weight restraints of MAVs [5]. This becomes increasingly true as the size of the MAV decreases.

Although rotary-wings are not common in nature, studies have been conducted to optimize rotor blade performance at low Reynolds numbers based on parameters such as solidity, twist, taper, camber, and tip shape [6, 7]. Overall, more progress needs to be made in basic understanding of low Reynolds number flight and utilization of natural flight aerodynamic phenomena.

1.1.2 Propulsion

Propulsion systems remain a limitation of MAV progress. Most current MAVs are electric-powered. Electric-powered systems efficiently convert stored energy into usable energy, but current battery technology has a low energy density. Gasoline has a very high energy density; however, internal combustion engines are highly inefficient at the MAV-scale and generate large noise signatures. Current propulsion systems available for MAVs are not suitable for long endurance, allowing less than 10 minutes of flight in many cases. MAV endurance is limited primarily by the efficiency of the system (figure of merit), and by the propulsive efficiency. Rotary-wing MAVs are especially limited in endurance because they inherently consume large amounts of power in order to hover. While electric power is currently the prevalent option for MAVs, research continues to refine and expand both propulsion arenas [1].

1.1.3 Flight Controls and Navigation

Low Reynolds number aerodynamics and the small size of MAVs make vehicle control more involved. Birds and insects use a variety of subtle movements, not only to produce lift, but also to control their flight direction. MAVs need miniaturized actuators and electronic devices that can serve as effective control devices. Current small actuators come in two basic categories: mechanical servos and magnetic servos. The smallest mechanical servo commercially available is the Falcon Mk III, which weighs 1.6 g and measures 21 mm in length [8]. Magnetic servos are smaller, with Plantraco's HingeAct magnetic actuator weighing only 0.22 g [9]. Traditional actuators are prohibitively heavy and require too much space as MAVs become increasingly smaller. A new area of research focuses on micro-electro-mechanical systems (MEMS). MEMS could allow integration of micro actuators, sensors, and electronics on a single device by using the techniques of integrated circuit fabrication. Once this technology develops, it can be exploited for MAV control design.

MAVs inherently suffer from control degradation because of their low wing loadings and inertial forces, which are stabilizing factors on full-scale aircraft. Because of the size of MAVs, perturbances such as wind gusts cause significantly large disturbances. A successful MAV will require a sophisticated stability and navigation suite in order to be able to survive gusty wind conditions and avoid obstacles in unfamiliar territory. Without an auto-stabilizing system, pilots in the field will be burdened by the constant attention required by marginally stable MAVs. Current navigation methods, such as GPS and inertial navigation systems, are either too heavy, require too much power, or need brand new technology to make their use on MAVs feasible [1]. The smallest commercially-available autopilot is Procerus Technologies' Kestrel [10], weighing 16.65 g and measuring 2 inches in length. The Kestrel provides GPS-based navigation, an inertial measurement unit for stability, payload communications, and data logging. However, this autopilot is prohibitively heavy for MAVs that weigh less than 100 g.

In order to reduce the weight of autopilot systems, innovative research is being conducted that utilizes optic flow methods for navigation. Optic flow refers to the apparent visual motion relative to an object in motion itself. Conroy et al. [11] are developing a system based on insect navigation that would also provide automatic landing. However, MAVs utilizing this system would still need to carry cameras for surveillance. Stuerzl et al. [12] are investigating a lightweight vision system that would provide both navigation and surveillance. Barrows et al. [13] are developing an optic flow sensor that can function in a real-world environment, which was tested on a small balsa wood and Styrofoam glider and on a 1-m wingspan remote-control aircraft.

1.1.4 Communications

MAVs need a communications suite in order to transmit mission data back to a central ground station. The problems associated with communication are largely due to the small size of MAVs. The size of the antenna is limited, as is the power available to support communications. An omni-directional antenna could provide the necessary range desired for an MAV, but its signal would be too weak because of the limited power available. Alternatively, a directional ground antenna requires less power, but would limit the MAV to line-of-sight tracking. By limiting the MAV to line-of-sight tracking only, the MAV would not be able to communicate over obstacles or from confined or densely populated areas—severely inhibiting its usefulness. Current wireless communication technologies, such as Bluetooth or WiFi, cannot provide the range necessary for MAV communications. Additionally, the current systems available cannot provide the 2-4 Megabits per second rate required for reconnaissance photo transmission. However, progress is being made in the cellular technology industry that may lead to adequate MAV communications systems [1].

1.1.5 Multi-function Subsystems

The size of MAVs requires that all systems on board be designed as lightweight structures able to withstand the anticipated loads. Current lightweight materials used in the construction of MAVs include wood, composites (often carbon fiber or fiberglass), and flexible membranes (such as Mylar). The flexible membranes are commonly used either as lightweight wing skins or coverings for the empennage or fuselage. Aluminum, steel, or titanium might also be used in small doses where strength is of particular importance.

If a component can be built such that it is multi-functional, then it would save weight, allowing the MAV to carry more payload, or extend its range or endurance. DARPA is investigating the monopolar proton exchange membrane fuel cell, which functions as both a wing skin and fuel cell. The metal grid that connects the membrane fuel cells is also multi-functional—it can be used as an antenna [14]. Telcordia's lithium-ion battery technology was recently developed into an aerodynamic wing shape for use on Aerovironment's WASP MAV [15]. Other multi-function systems are also under development.

1.2 State-of-the-Art

The following sections describe recent research efforts that have examined MAVs.

1.2.1 Fixed-Wing MAVs

While the small size of MAVs is enticing, there are associated technology barriers. The most apparent are the difficulty associated with miniaturization and our limited understanding of the complex low Reynolds number aerodynamic regime where MAVs operate. Studies [16, 17, 18] in fixed-wing aerodynamics have explored the effects of low Reynolds number flight. The results showed that airfoil performance deteriorates due to lower maximum lift coefficients, stall occurring at lower angles of attack, and increased drag coefficients due to laminar separation bubble effects. Nevertheless, the most advanced MAVs to-date are of the fixed-wing variety, where much work has been done by modelers and researchers alike.

Torres and Mueller [19] studied a variety of flat-plate, fixed-wing planforms for MAV applications. The models had a thickness-to-chord ratio of 1.96%, and elliptical leading and trailing edges. Wind tunnel tests were conducted on rectangular, elliptical, circular, and Zimmerman-shaped (conjoined ellipses) planforms. A total of 12 planforms were tested, with aspect ratios ranging from 0.5 to 2. Lift and drag were measured for each of the planforms at angles of attack between -15° and 30° in 1° increments. Results showed that the lift versus angle of attack curves became increasingly nonlinear at high angles of attack. The stall angle of attack increased as the aspect ratio decreased. For aspect ratios less than 1.0 and a Reynolds number of 100,000, the rectangular and inverse Zimmerman planforms were found to be most efficient.

AeroVironment developed the widely successful Black Widow, a 6-in span, fixed-wing MAV for phase one of DARPA's micro air vehicle initiative [20]. Multidisciplinary design optimization was employed to determine the battery, motor, gearbox, power requirements, propeller diameter, wingtip chord, and cruise velocity combination that would result in the best configuration. The platform was then designed to deliver live images in real-time via a custom-made color camera and transmitter. Development of the Black Widow MAV showed that direct-drive propulsion systems were more efficient for a fixed-wing vehicle, propeller efficiencies of greater than 80% were possible, motor efficiencies of greater than 70% were possible, and electric-propulsion systems were the best currently-available option for MAV applications. The Black Widow had a video transmit range of 1.8 km and an endurance of 30 minutes. Research from the Black Widow developed into AeroVironment's WASP MAV, a response to DARPA's phase two MAV initiative. The WASP utilizes multifunction structure - energy storage components [21]. In August of 2002, the WASP set a record for MAV endurance with a flight duration of 1 hour 47 minutes [9].

Figure 1.3: AeroVironment WASP [21]

Abdulrahim et al. [22, 23] have recently developed fixed-wing MAVs that implemented various forms of biologically-inspired morphing techniques. Morphing implies that the aircraft changes shape during flight to optimize performance. Most often occurring in wings, morphing can include changes of span, camber, chord, aspect ratio, thickness, or planform area. At the time of their research, many fixed-wing MAVs were being designed with membrane wings, which made it difficult to include ailerons for roll control. Thus, many MAVs had only a rudder and elevator, for yaw and pitch control respectively. To remedy the lack of ailerons, the use of morphing as an aeroservoelastic effector for roll control was investigated. In this case, the type of morphing investigated was wing twisting. A fixed-wing MAV of 24-in wingspan weighing 13.4 oz was designed. Single-surface wings were built of a composite carbon fiber skeleton with a plastic covering that could be easily morphed mechanically. Torque rods were connected to independent servos in the fuselage and, when actuated, were able to control wing twist. Flight tests demonstrated sufficient control authority using these morphing, membrane wings.

Another fixed-wing MAV is called the MLB Trochoid [24]—it utilizes a trochoidal planform to maintain control effectiveness in highly vortical flow conditions. The Trochoid had a 20-cm maximum dimension and was able to fly for 20 minutes at speeds up to 60 mph. The elevator and rudder were the only control surfaces necessary due to high yaw-roll coupling.

The University of Florida developed flexible-wing design MAVs [25]—which employed highly flexible wing skins. These MAVs had a wingspan of 16 cm, and were used for wind tunnel testing to examine the effects of three internal flexible membrane structures: a rigid carbon fiber structure, a flexible structure with carbon fiber battens, and a flexible structure with carbon fiber perimeter. Measurements of lift, drag, and pitching moment were collected for a range of angles of attack, airspeeds, and throttle settings. A simulation model was developed from the data to assist future studies of the MAVs pictured in Figure 1.4.

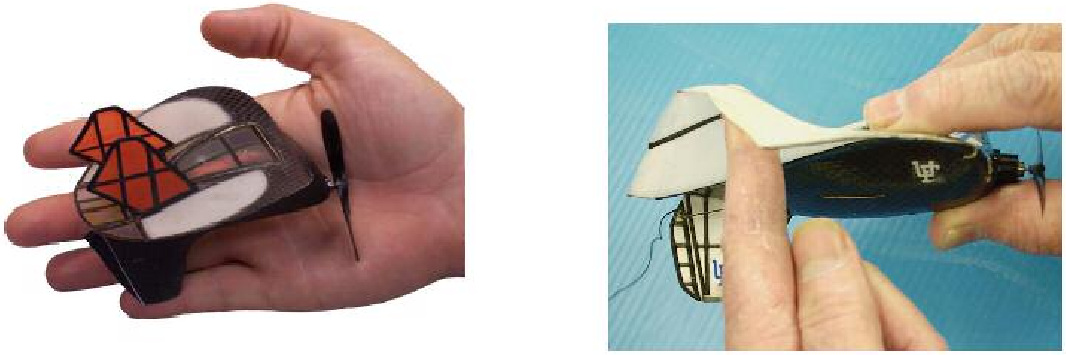

Figure 1.4: University of Florida Flexible-Wing MAVs [25]

The University of Arizona has developed several 6- to 12-in span fixed-wing MAVs, and has competed in several MAV competitions. Their smallest MAV to-date utilized a camber-with-reflexed-edge airfoil, and had only elevator and rudder control. Recent research at the University of Arizona has focused on reflexed-edge airfoil optimization for their MAVs. Wind tunnel tests were performed on 8-in span MAV models with 3% to 12% camber, and results indicated that the 3% cambered airfoil performed best in high speed flight, whereas the 9% cambered airfoil performed best in slow flight [26, 27].

Despite the abundance of ongoing research, fixed-wing MAVs are not suitable for operations in constrained areas because of their relatively high stall speeds. Thus, researchers have begun to investigate rotary and flapping-wing MAV designs, which can safely operate at low speeds and offer the potential to hover. However, unlike fixed wings, these MAVs operate in a more complex aerodynamic environment.

1.2.2 Rotary-Wing MAVs

Helicopter MAVs are enticing because of their ability to hover, and have been built and studied by many. Unless carefully designed, rotors can suffer from performance degradation at low Reynolds numbers because their airfoils operate in a more challenging environment. Scaling down rotor blades and using low Reynolds number airfoils results in figures of merit in the range of 0.4 to 0.5, a value far less than the full scale value of about 0.8. Thus, alternative avenues (novel configurations, ducted designs, new airfoils) need to be explored in order to achieve a competitive figure of merit [28, 29].

Researchers at Stanford University [30] developed the Mesicopter, a meso-scale quad-rotor electric helicopter that operated at a Reynolds number of approximately 5000. Each of the four rotors of the Mesicopter had a diameter of 1.5 cm, and the total weight was 3 g. Varying the torque on the motors separately allowed the Mesicopter to maneuver using roll, pitch, yaw, and thrust. The Mesicopter was powered via lithium polymer batteries using a tether. Emphasis was placed on aerodynamics and manufacturing processes in order to demonstrate the Mesicopter as a successful concept.

Figure 1.5: Mesicopter Rotary-Wing MAV [31]

Two micro helicopters have been developed at the University of Maryland: a single rotor with active turning vanes [32], and a coaxial rotor system [33, 34]. The single rotor with turning vanes is a 2-bladed, teetering hinge, ducted rotor, with a diameter of 25 cm. It utilizes turning vanes placed under the slipstream to counteract the torque of the rotor. Control surfaces on the vanes control yaw of the vehicle, and a swashplate provides lateral control. The vehicle has a total weight of 240 g. The concept has flown successfully and is currently being updated with a small inertial measurement unit for stability augmentation. The micro coaxial rotor system (MICOR) developed at the University of Maryland has two counter-rotating rotors of 9-in diameter, weighs 145 g, has a payload capacity of 20 g, and an endurance of 10 min. The two counter-rotating rotors negate the need for a tail rotor, which allows the design to be more compact. Significant effort was put into the rotor blade design of MICOR, resulting in a figure of merit increase from 0.42 to 0.64 by investigating the effects of airfoil camber, leading edge shape, and blade tip shape. MICOR also incorporates an innovative swashplate design, which provides good longitudinal and lateral control at a minimum weight. The University of Maryland micro rotorcraft exemplify the utility of such designs, and are pictured in Figure 1.6 and Figure 1.7. Their ability to hover is their most significant advantage; however, this comes at a high cost in terms of power required. Large power requirements translate into a lower endurance, lower payload capacity, and limited flight speeds compared to fixed-wing MAVs.

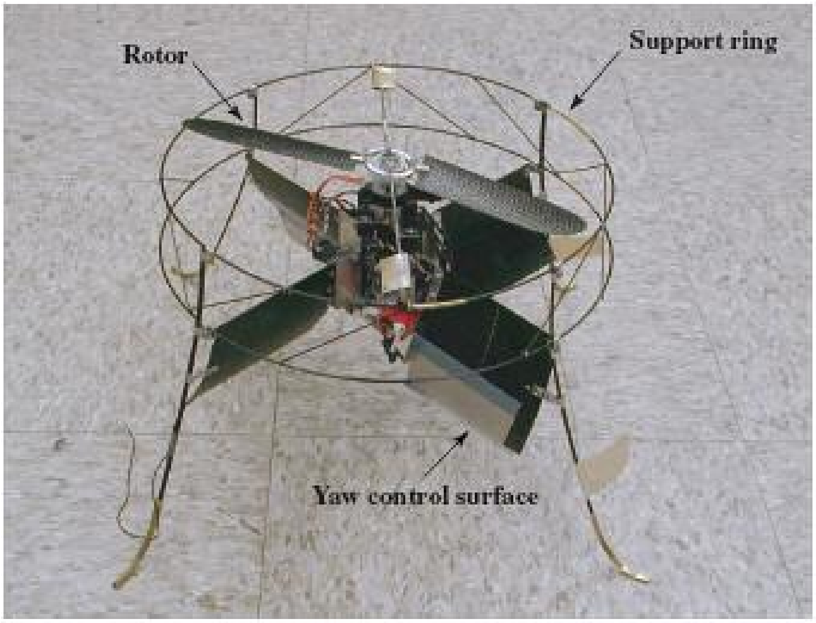

Figure 1.6: Single Rotor with Turning Vanes [32]

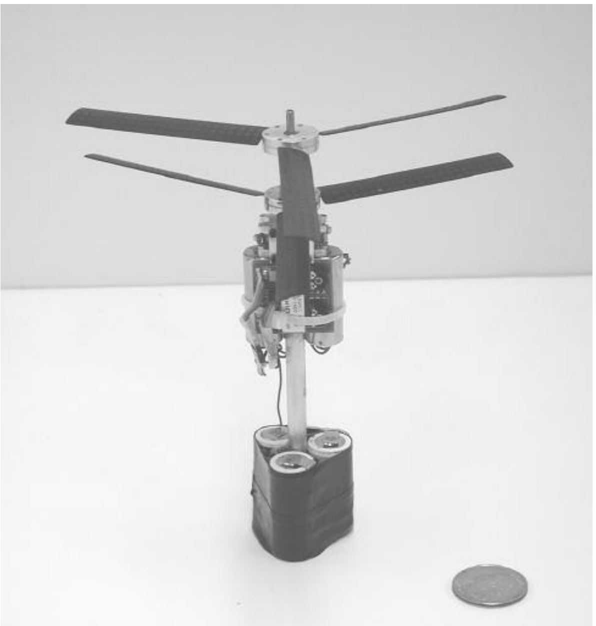

Figure 1.7: MICOR Prototype [33]

1.2.3 Flapping-Wing MAVs

For the small scale of MAVs, flapping wing vehicles may be the preferred approach because of their abundance in nature, and their ability to harness low Reynolds number unsteady vortex lift effects. Flapping wings can blend more naturally into the outdoor environment, providing camouflage—and there is a wealth of biological inspiration to draw upon. Flapping-wing MAVs come in a variety of shapes. Some are based on avian flight, whereas others are based on insect flight. Some have traditional airfoils for wings, and others have thin membrane wings. Some can hover, and some employ unusual mechanisms of lift.

Insect-Based MAVs

Insect-based MAVs offer the advantages of being small and having the potential to hover; however, because they operate at low Reynolds numbers where viscous effects dominate, they require high flapping frequencies and consume large amounts of power. Their small size also restricts their payload capacity. Additionally, the highly evolved motions involved with insect flight renders mechanical replication difficult and costly in terms of weight.

Insect wingstrokes differ from avian wingstrokes because the wings quickly rotate and reverse direction between the upstrokes and downstrokes. Insects use this motion to produce lift based on three mechanisms: delayed stall, rotational circulation, and wake capture. During the upstroke and downstroke, the insect wing is at a high angle of attack, which causes a leading edge vortex to form. When the wing flips at the end of the stroke, a new vortex forms in the opposite direction. The tip vortex prevents the leading edge vortex from growing large enough to shed, so it remains attached to the wing—augmenting lift. This process is referred to as delayed stall. Rotational circulation occurs at the end of each upstroke and downstroke when the wing flips to change direction. This rotation provides additional circulation, which augments the lift. Wake capture also happens during the wing rotation. At the beginning of each stroke, the wing passes through the wake of the previous stroke such that the increased airflow adds additional lift.

Insects that do not rotate their wings at the end of each upstroke and downstroke utilize the clap-fling mechanism, discussed earlier. Despite the complexities and limitations associated with insect flight, MAVs have been developed based on both the clap-fling mechanism and rotational lift mechanisms.

Jones et al. [35, 36, 37] have recently conducted experimental and computational investigations of clap-fling propulsion mechanisms for flapping-wing MAV applications.

Various combinations of pitch and plunge oscillations of single and combined airfoils were considered, and resulted in some unique MAV design concepts, such as the NPS Flapping-Wing MAV. The NPS Flapping-Wing MAV measures 25-cm in span, 15-cm in length, and uses pure pitch motion to clap two flexible wings together at 32 Hz. The flapping wings were located aft of a larger, fixed wing that produces lift. As the wings flapped together, the clapping motion produced thrust via the clap-fling mechanism. The flapping wings also suppressed flow separation on the fixed wing, preventing stall. Since the wings flapped counterphase, the fuselage remained steady. The NPS Flapping-Wing MAV weighed 12.4 g, had only rudder and throttle control, and could fly for 20 minutes using Lithium Polymer batteries. The vehicle demonstrated how the lift and thrust mechanisms of insect flight could be utilized in a simplified manner.

Another design based on the clap-fling mechanism was MENTOR [38] – developed at the University of Toronto’s Institute for Aerospace Studies. MENTOR had a 30-cm wingspan, two sets of wings, and weighed 550 g. MENTOR could fly for 10 min, but because of the clapping of its wings, had a large noise signature. MENTOR was the first flapping-wing aircraft to hover under its own power.

Another insect-based flapping-wing MAV that is under development is Vanderbilt’s Elasto-Dynamic Ornithoptic Robotic Insect—which utilizes piezoceramic-actuated vibrating wing structures [39]. UC Berkeley is developing the Micromechanical Flying Insect [40]. The Micromechanical Flying Insect employs insect-based phasing between wing flapping and rotational motions in order to achieve flight control. The design goals require a mass of 100 mg, wingspan of 25 mm, and flapping frequency of 150 Hz.

Additional research is underway at the University of Maryland. Singh et al. [41] used a flapping-wing test apparatus capable of emulating insect kinematics (active flapping and pitching) to test various planforms and materials. Rectangular planforms and scaled-up fruit-fly planforms were tested. Wing structures were constructed of aluminum, carbon composite, or fiberglass. Wing skins were constructed of Mylar or RC Microlite. Thrust and power measurements were collected between 6 and 24 Hz. Results indicated that a high wing mass restricted attainable frequencies, and that thrust decreased at high frequencies. Thrust was higher for wings utilizing passive pitching. Tests were conducted with soft and stiff torsion springs for passive pitch, and results indicated that the soft torsion spring allowed greater thrust production and a greater range of pitch variation.

Tarascio et al. [42] conceptualized a hybrid, insect-based MAV called the Thrust Augmented Entomopter (TAE). The configuration utilized flapping wings to hover, and a pusher propeller for thrust in forward flight. The wings would be configured for minimum power requirements in hover, and would not flap during forward flight. The concept had an estimated weight of 160 g, and a wingspan of 218 mm.

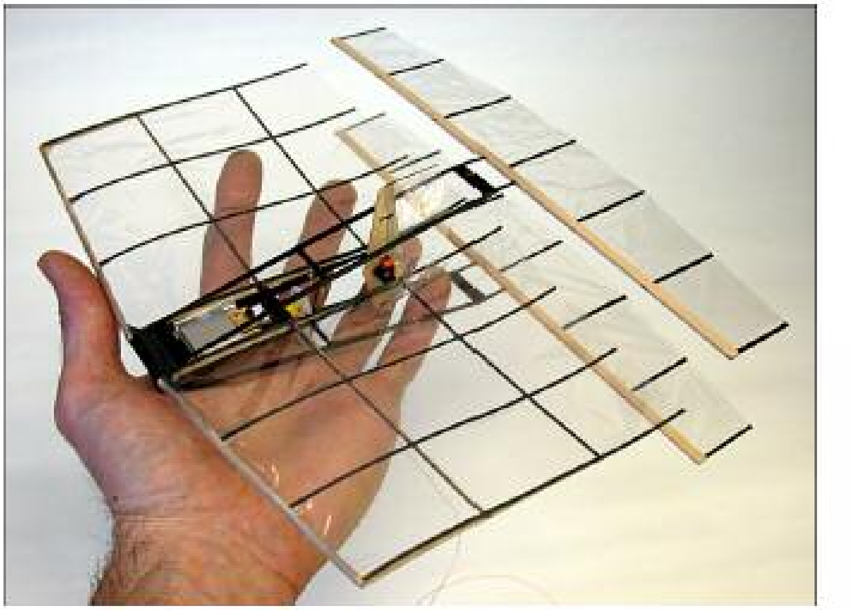

Figure 1.8: NPS Flapping-Wing MAV [32]

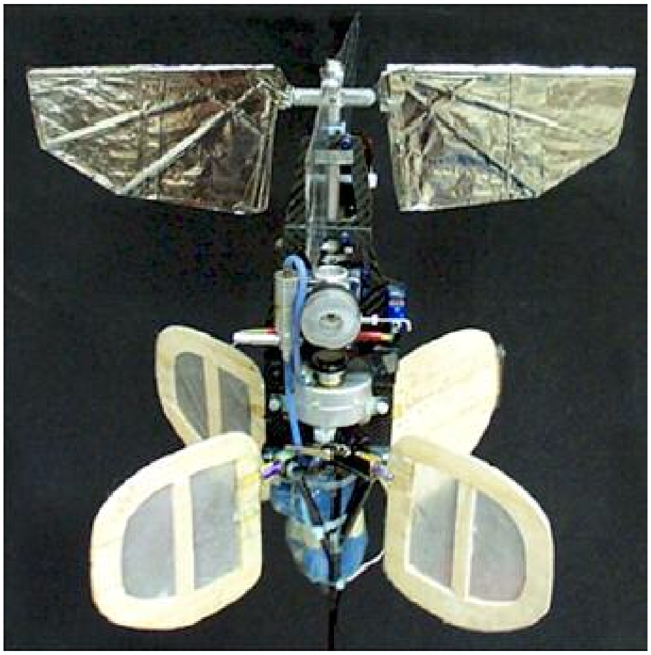

Figure 1.9: MENTOR Flapping-Wing MAV [43]

Avian-Based MAVs

The challenge of designing flapping-wing vehicles is simulating nature's highly evolved wing movements into simpler, mechanical ones that still make use of the lift mechanisms of avian flight. The advantage of employing avian-based flight is that the aerodynamics can be simplified by using simple up-down flapping motion with flexible membrane wing skins. The use of a flexible membrane allows the wing to passively change its relative angle of attack and camber during the stroke cycle. This is the mechanism by which commercially-available ornithopters operate. Although this simplification is adequate for producing lift and thrust, birds still have an advantage in their ability to adjust their flapping scheme for different flight regimes. Thus, research continues on how to incorporate more aspects of avian flight.

Though rubber band-powered ornithopters have been around for hundreds of years, the advent of engine-powered ornithopters began in the late 1980s. DeLaurier [44] studied the drag and leading edge suction of cambered airfoils, and subsequently developed the first aerodynamic model to accurately predict flapping wing behavior. In 1991, DeLaurier and Harris used that aerodynamic model to design and launch the first engine-powered ornithopter that could sustain flight. Their ornithopter was ¼ scale, had a cruise speed of 34 mph, flapping frequency of 3 Hz, and payload capacity of 8 oz. The ornithopter used an S1020 airfoil, which was designed to have attached flow over a wide range of angles of attack [45, 46].

Figure 1.10: The First Successful Engine-Powered Ornithopter [27]

Since DeLaurier’s historic flight, ornithopter development has continued. Most recently, ornithopters have been the focus for MAV design, largely because they do not have the high power consumption of rotary-wing MAVs, and because they are more maneuverable at slow speeds than fixed-wing MAVs. Additionally, ornithopters offer the potential ability to hover.

Pornsin-sirirak et al. [47] developed super-capacitor and battery-powered flapping-wing MAVs based on MEMS technology. A titanium-alloy metal wingframe and flexible, parylene-C wing membrane allowed design of a free flight super-capacitor powered MAV weighing only 6.5 grams, which flew for a duration of 9 seconds. The battery-powered MAV weighed 10.6 g, and flew for 18 seconds. Both MAVs had a wingspan of 14 cm.

The most notable flapping-wing MAV yet developed (largely because it was one of the first) was AeroVironment’s Microbat [48]. The Microbat was a 23-cm span, electric-powered ornithopter, developed in response to DARPA’s original MAV initative. Microbat was built primarily of carbon fiber and Mylar, weighted 12.5 g, had an endurance of 22 min, and was remotely piloted. Microbat was controlled with traditional rudder and elevator tabs on a conventional tail structure.

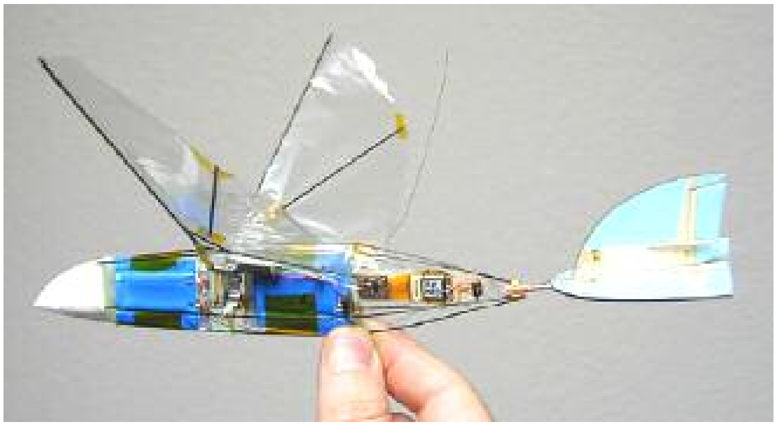

Figure 1.11: Microbat Flapping-Wing MAV [15]

Another ornithopter recently developed was the DelFly [49]. The DelFly had two sets of flapping wings, which allowed it to fly both fast forward flight missions and very slow, loitering missions. It had a 350 mm wingspan, flapping frequency of 6 Hz, and weight of 17 g. The rudder-vators of the V-tail were actuated by shape memory alloy wires. The DelFly carried a video camera payload, allowing it to recognize targets. It had an endurance of 12 minutes at a cruise speed of 1.8 m/s.

Figure 1.12: DelFly Flapping-Wing MAV [49]

At the 9th International Micro Air Vehicle Competition in 2005, the University of Arizona (UA) took 1st place for their 9-in span ornithopter design [26]. Rankings were based on size and the number of flaps the ornithopters around a pylon course in a two minute timeframe. The UA ornithopter had a flapping frequency of 20 – 22 Hz, and was constructed primarily of carbon fiber, balsa wood, and mylar. The University had also constructed a 7-in span ornithopter, but chose not to fly it at the competition.

Despite these successful efforts, ornithopters require continued research in order to reach longer endurances and utilize more efficient lift mechanisms. Some recent research has begun to examine these aspects of flapping wings.

Frampton et al. [39] investigated flapping wing twist and bending to optimize designs via aeroelastic tailoring. A test bed was built to measure thrust forces and power consumption of several wing designs. All wings were a rectangular, Mylar planform of 6-in span and had an aspect ratio of 2.3. Variation of spar width and thickness allowed for aeroelastic diversity. The wing natural frequencies of bending and torsion were passively tailored in this way. The results showed that a wing employing in-phase bending and torsion modes created the most thrust, whereas if the torsion mode lagged bending by 90º the best efficiency was achieved.

Flapping-wing shape optimization was also examined by Pornsin-sirirak et al. [47], who studied Titanium-alloy MEMS wings with elliptical, beetle, dragonfly, bat, and butterfly planforms. Photolithography was utilized for wing construction, and wind tunnel tests were conducted. Construction materials, chord width, spar width, membrane thickness, number of spars, and sweep angles were varied. Tests were carried out at flapping frequencies up to 30 Hz at wind tunnel velocities between 1 m/s and 10 m/s. The results indicated that a MEMS wing of polynomial planform showed the best performance. A key observation was that the complicated nature-based planforms performed poorly compared to simpler planforms.

Malolan et al. [50] studied six flexible, flapping-wing planforms of polyethylene construction. Each of the 15-cm span wings was tested for lift generation at a variety of freestream velocities for flapping frequencies ranging between 8 Hz and 16 Hz. A wing with a high aspect ratio outboard section and large inboard chord showed the best performance. Similarly, Muniappan et al. [51] studied the lift and thrust characteristics of flexible, varying aspect ratio elliptical planforms, as well as dragonfly, butterfly, hummingbird, and pigeon-based planforms. Wind tunnels tests were conducted at flapping frequencies of 4 Hz to 20 Hz, at freestream velocities of 1 m/s to 5 m/s. The planforms varied in span, and had aspect ratios ranging from 3.3 to 8.1. The butterfly planform (aspect ratio of 3.3) was found to be most effective.

Flapping-wing comparisons were also carried out by Ho et al [52]. Wings of 7-cm span with and without inboard root sections were compared, as were rigid wings versus flexible wings. Wind tunnel tests were carried out at a variety of flapping frequencies and freestream velocities. The results showed that more flexible wings were able to produce thrust, whereas rigid wings were not, and wings with inboard root sections could produce more lift and thrust over a range of velocities. A MEMS-based wing with check-valve electrostatic actuators was developed and tested as a result. The check-valve actuators were placed near the leading edge, where they would be most effective. The check valves closed during the downstroke and opened during the upstroke, mimicking the way birds can adjust their feathers during the upstroke to reduce drag. The use of the actuators resulted in an average lift increase of 31%, and an average thrust increase of 17%.

1.3 Contribution of the Present Work

This paper seeks to improve upon current flapping-wing performance by incorporating the effects of nonplanar wings. The motivation for including nonplanar tips is based on the several factors. First, nonplanar tips have been shown to provide slight increases in thrust in fixed-wing aircraft. Second, avian flight indicates that twisting or folding the wings on the upstroke will reduce the amount of negative lift generated. Third, model ornithopter builders [56] have discovered that the use of curved spars can contribute additional lift during the upstroke.

In this study, lift and thrust tests were conducted on various wing planforms with nonplanar tips, where the nonplanar effects were investigated with varying degrees of wing tip arcs and tip anhedral. Based on the results, a prototype flapping-wing MAV was developed and tested.

1.4 Thesis Outline

This thesis is composed of five chapters. A brief description of the chapters follows:

1. **Chapter 1 : Introduction:** A description of the problem statement, the previous work on the topic, and the contribution of the present work is presented.
2. **Chapter 2 : Physical Principles:** This chapter deals with the physical principles that govern low Reynolds number aerodynamics and flapping wing flight. Methods for predicting lift and drag of flapping wings are discussed.
3. **Chapter 3 : Experiments:** This chapter presents the wind tunnel measurements of lift generated by elliptical and polynomial planforms with varying degrees of tip anhedral. Experimental results are discussed and applied to the MAV designed herein.
4. **Chapter 4 : Explanation of Results:** The instantaneous lift of planar and nonplanar wings are compared. A strobe analysis is performed to investigate wing membrane deformations at various stages of the flap cycle.
5. **Chapter 5 : Conclusions and Future Work:** Important conclusions are drawn from the experiments, leading to suggestions for future flapping-wing MAV development efforts.

Chapter

2 Physical Principles

The physical principles associated with low Reynolds number aerodynamics and membrane-wing flapping flight are discussed below. Theoretical methods for analyzing flapping flight are also discussed.

2.1 Low Reynolds Number Aerodynamics

As discussed in Chapter 1, MAVs operate in a low Reynolds number flight regime. The Reynolds number is a common ratio of inertial to viscous forces in aerodynamics, and is defined by Equation 2.1.

$$\mathrm{Re} = \frac{Inertial}{Viscous} = \frac{\rho S V^2}{\mu S V / l} = \frac{\rho l V}{\mu} \tag{2.1}$$

where ρ is the fluid density, l is a characteristic length, V is the fluid velocity, and μ is the dynamic viscosity of the fluid.

While full-scale aircraft generally have Reynolds numbers greater than 1,000,000, MAV Reynolds numbers will be less than 100,000. At low Reynolds numbers, the flow environment is laminar and highly viscous. This means that vortices are more difficult to sustain and that velocity gradients are very gentle unless large forces are applied. Because of this viscous flow environment, streamlined shapes—such as airfoils—are increasingly enveloped in a thick boundary layer, inhibiting their ability to generate lift. Due to greater skin friction, the profile drag increases. Consequently, the lift-to-drag ratios (L/D) of airfoils at low Reynolds numbers drop significantly. [53]

In 1938, Goldstein [54] performed studies of airfoils at low Reynolds numbers. An airfoil at a Reynolds number of 6,500,000 had an L/D of 60, whereas the L/D of the same airfoil was 47 at 310,000 Reynolds number. The stall angle was also found to decrease as Reynolds number decreases. The stall angle of an airfoil decreased from 18º at 3,300,000 Reynolds number, to 12º at 330,000, and to 9º at 43,000. In 1960, Schmitz [55] considered the design of model airplane airfoils, and found that a moderately cambered flat plate with a thickness-to-chord ratio of 5% performed better than conventional airfoils at a Reynolds number of 42,000. At a Reynolds number of 168,000, the conventional airfoil performed better in all respects.

Thus, many of the MAV examples cited in Chapter 1 did not employ conventional wings and airfoils—nor did the prototype developed herein.

2.2 Lift and Thrust of Flapping Membrane Wings

Conventional airplanes have wings and engines to separately produce lift and thrust, whereas flapping-wing aircraft produce both lift and thrust with only the wings. For flexible membrane-covered flapping wings, each wing flaps up and down, causing the membrane to automatically change pitch and camber with the relative flow. The flexibility of the membrane will determine the amount of pitch and camber of the wing. These passive membrane changes create forces that vary throughout the flap cycle. Positive lift is produced on the downstroke, and negative lift is produced on the upstroke. If the upstroke and downstroke are identical, then the net lift is zero. This process is simplistically illustrated in Figure 2.1. [56]

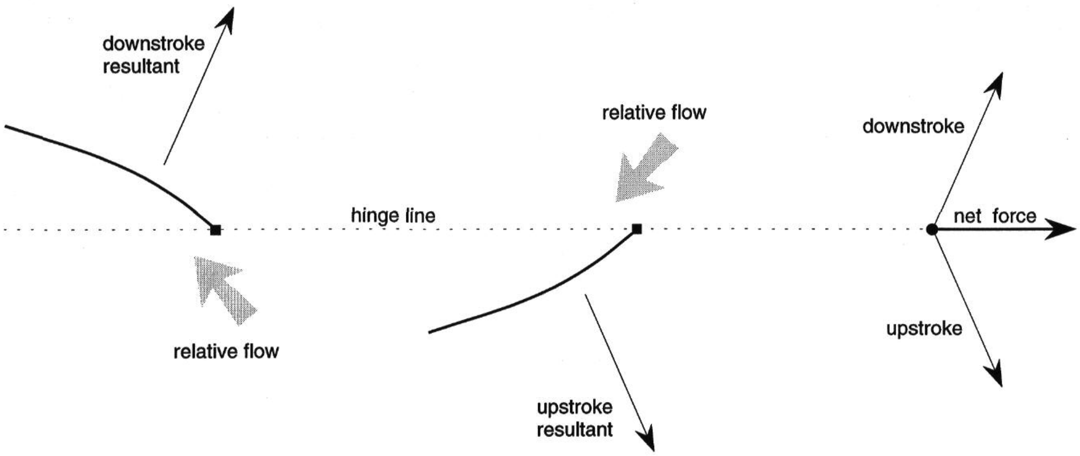

Figure 2.1: Forces Created by a Flapping Membrane Wing [56]

If the hinge line is rotated such that it sits at a positive pitch angle, then the net force will be vectored—resulting in both lift and thrust. While this is a simple way to explain flapping-wing lift and thrust, it is not entirely accurate. To fully understand flapping wings, the spanwise variation in flow must be considered.

The inboard section of a flapping wing is close to the wing hinge point, so there is comparatively little up and down movement. If the hinge line has positive pitch, then the inboard section of the wing will act much like a fixed-wing—producing positive lift. As the magnitude of vertical movement increases from the root outward, the resultant forces change because of passive twisting and cambering of the flexible membrane. The downstroke resultant force will gradually tilt forward as it progresses from root to tip. Drag is produced on the inboard section, and thrust is produced near the tip. The upstroke produces lift near the root, but at some point along the span the upstroke resultant causes negative lift because of the negative camber that has been induced by the membrane. At that point only drag is being produced. Further outboard, the upstroke continues to produce negative lift, but begins to produce positive thrust because of passive twist. The spanwise variation of forces is depicted in Figure 2.2 [56].

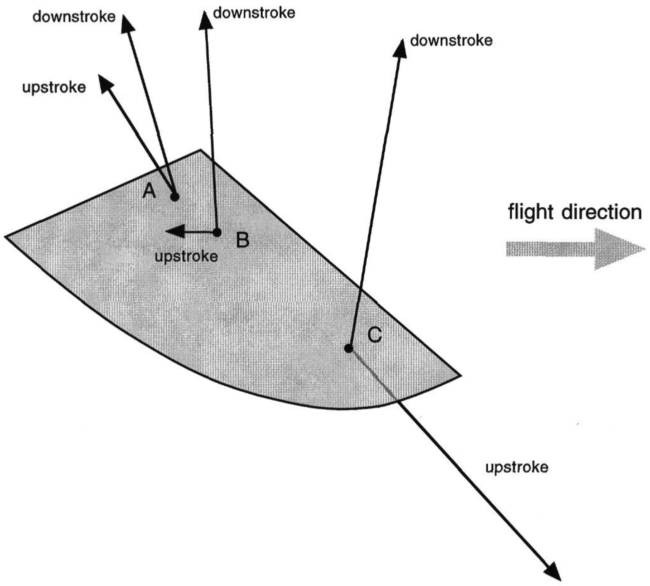

Figure 2.2: Spanwise Variation of Flapping-Wing Forces [56]

Though effective and simple to construct, there is a drawback to using membrane wings. As discussed previously, at the top and bottom of the flap cycle the membrane reverses its camber. During this reversal, the membrane becomes limp and cannot produce any useful force. Therefore, during a sizeable portion of the flap cycle, the wing is wasting energy. There have been recent attempts to increase upstroke lift and maintain membrane tension throughout the turnaround. These methods included spring-loaded downstrokes, aeroelastically tailored wings, or the use of mechanical devices connected to the flapping mechanism [56].

2.3 Predicting Flapping Wing Forces

There are two primary approaches to predicting flapping-wing forces: blade element analysis and the theory of the wake.

2.3.1 Blade Element Analysis

During a study of the migratory desert locust in the 1950's, biologists Weis-Fogh and Jensen [57] set out to predict the aerodynamic forces produced by the wings. Borrowing a technique from helicopter theory, they were the first to use blade element analysis on flapping wings.

In blade element analysis, the wing is treated as a set of spanwise strips, starting from the root. On each strip, the local freestream velocity and angle of attack can be determined geometrically from the flight speed of the vehicle and the flapping frequency of the wings. The resultant local velocities and angles of attack are used to calculate the lift and drag on each strip according to steady aerodynamic definitions. Summing the lift and drag over all of the strips results in the overall lift and drag at any instant. In order to calculate the average lift and drag over an entire wing-beat cycle, Weis-Fogh and Jensen performed blade element analysis for a large number of iterations during the stroke cycle and averaged these values. This approach is referred to as a quasi-steady analysis because it breaks down long, time-varying motions into a series of short, steady motions. [4]

2.3.2 Theory of the Wake

A vortex wake model is based on the theory that aerodynamic forces produced by flapping wings must be balanced by momentum changes in the surrounding air. The advantage of a vortex wake model is that the details of airflow and lift production on the wings are not of concern. Basic properties of the flapping cycle—such as wing length, flapping frequency, and amplitude—and the size and strength of trailing vortices can be used to calculate the aerodynamic forces. [4]

2.3.3 Studies in Flapping-Wing Computational Fluid Dynamics (CFD)

With the advent of CFD, not only have lift and thrust prediction methods improved, but many new computational studies have taken place and are becoming increasingly sophisticated. Of particular interest to the research herein is work done by Ho et al. [52], which focused on the planform shape optimization of membrane flapping-wings. An aeroelastic computational study of flexible membrane versus rigid wings was conducted. The computational analysis incorporated a commercially-available Navier-Stokes CFD package, finite element analysis, and the Gur Game feedback control algorithm into a single simulation. The program optimized wing stiffness distribution for lift and thrust production simultaneously. Lift was defined in the direction perpendicular to the freestream velocity, whereas thrust was defined parallel and into the freestream velocity. The model was validated with experimental test data of fully flexible MEMs wings. The average lift and thrust results plotted versus freestream velocity are reproduced in Figure 2.3. Key conclusions of the computational study were that wings must be highly flexible in order to produce both lift and thrust, that optimized wingtips were stiffer than the membrane, and that optimized wings do not create larger forces, instead they decrease adverse forces.

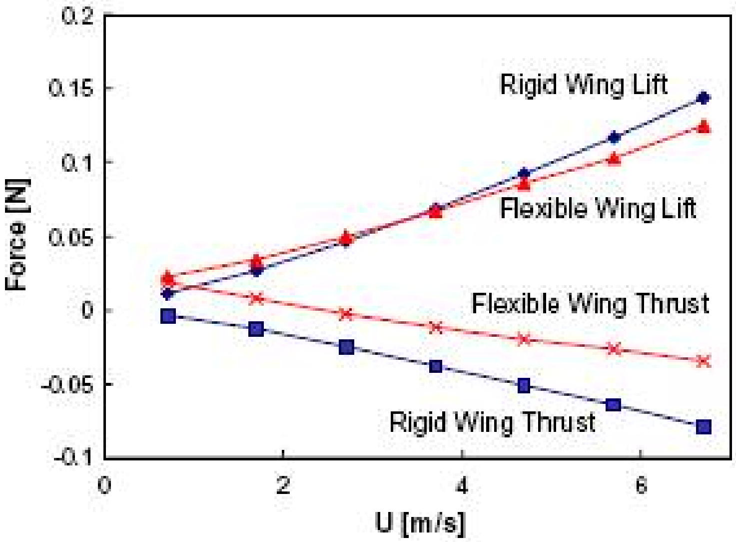

Figure 2.3: Computationally-Derived Rigid and Flexible Wing Lift and Thrust [52]

Chapter

3 Experiments

3.1 Objectives

The objective of this research is to design a flapping-wing MAV prototype based on experimental optimization of membrane wing planforms, including nonplanar planforms. The approach to meeting the objective is: to perform a proof-of-concept investigation of nonplanar wing types, to design and manufacture a prototype flapping-wing MAV, and to implement the prototype MAV for extensive wind tunnel testing of various membrane wing planforms, including nonplanar effects.

3.2 Experimental Approach

To compare the performance of a variety of wing planforms, lift and thrust values would need to be determined over a range of flapping frequencies. At the small scale of MAVs, lift and thrust measuring devices would need to meet the required precision and size constraints. However, in order to determine these constraints, it was necessary to first establish initial sizing of the vehicle. Initial sizing would provide estimates of lift requirements and flapping frequencies—allowing for proper selection of lift and thrust measuring devices.

3.3 Initial Sizing

A fixed span of 6-inches was chosen to ensure that the vehicle would meet the general size requirement for MAVs set by DARPA, then biological mimicry was used to size the experiments and MAV design concept. Initial sizing was determined by using geometric scaling factors for passeriforms cited in Norberg's Vertebrate Flight [58]. Based on the fixed span, the ideal mass, flapping frequency, wing area, and aspect ratio of the MAV were determined from the logarithmic relationships presented in Table 3-1. The resulting values were used as an initial starting point for design of a flapping-wing MAV. Norberg's scaling factors indicated that the MAV should weigh no more than 10 g, and have a flapping frequency of approximately 16-18 Hz.

Table 3-1: Initial Sizing for Conceptual Design of an MAV

Quantity	**Relationship**	**Result**
Wingspan, b (in)	Fixed	6
Mass, M (kg)	$M_{lower} = 0.606 b^{2.381}$	0.0069 to 0.0100
	$M_{upper} = 0.885 b^{2.381}$	
Flapping Frequency, f (Hz)	$f = 3.03 M^{-0.36}$	15.8 to 18.2
Wing Area, S (m^2)	$S_{lower} = 0.16 M^{0.78}$	0.0044 to 0.0068
	$S_{upper} = 0.33 M^{0.78}$	
Aspect Ratio, AR	$AR_{lower} = 7.83 M^{0.05}$	6.22 to 6.35
	$AR_{upper} = 8.15 M^{0.05}$	

3.4 Test Stand Experiment

To begin the detailed design of a flapping-wing MAV, a test was conducted to compare the amount of lift and propulsive thrust that could be generated by planar and nonplanar wing planforms of the same wingspan.

3.4.1 Test Stand Set-up

An aluminum test stand, powered by a small motor, was built to simulate simple vertical flapping motion with interchangeable wings. The test stand had a flat, rectangular aluminum base with four aluminum rods extending from each corner to a flat, aluminum top. At one end of the plate, a small generic motor was attached vertically with the motor shaft extending through the top plate. The motor shaft drove an aluminum circular disk of 1-in diameter. A connecting rod hinged from a point on the edge of the disk to a 0.25-in rotary arm at the opposite end of the plate. The rotary arm was securely attached to a 1/8-in aluminum shaft extending vertically from the plates. The movement of the circular disk causes the connecting rod to transfer motion to the rotary arm, which translates into a back-and-forth rotation of the shaft. Interchangeable wings could be attached at the top of the shaft to simulate simple vertical flapping motion. A wing attachment part was built for this purpose. The wing attachment was built from a 1-in long, 0.25-diameter aluminum rod. The center section of the rod was lathed to a diameter of 1/8-in. At one end, a 1/8-in hole was drilled vertically, where the shaft of the test stand would attach. A set screw held the attachment arm in place. At the other end of the attachment arm, a 0.05-in hole was drilled horizontally. Through this orifice, various wings could be attached and secured with a set screw.

A thin-film, F.W. Bell FH-301-series transverse Hall sensor was positioned underneath the circular disk, and a magnet was attached to the underside of the disk. This allowed measurement of the flapping frequency of the wings. A Midori CP-2UTX low-torque, contactless potentiometer was positioned at the base of the output shaft to record instantaneous angular position of the wing. The flapping amplitude of the wings varied from -10º at the bottom of the downstroke to +30º at the top of the upstroke. Entran ESU-025-500 strain gages were selected to measure the lift and thrust based on the initial sizing. They were small enough to mount on the arm of the test stand and they could provide the required precision of measurement for lift measurements in the range of 10 g. Two strain gages were mounted 90º apart on the center section of the wing mounting arm, allowing measurements of lift and thrust.

One strain gage was mounted chordwise to measure instantaneous propulsive force. The other strain gage was mounted perpendicular to the chord line, which measured the instantaneous force perpendicular to the wing. The average propulsive force was determined by summing the instantaneous chordwise forces for one complete flap cycle. By definition, the lift was the average force exerted on the wing throughout one complete flap cycle, directed perpendicular to the initial position of the wing (0º flapping amplitude). Therefore, the lift was determined by transforming instantaneous perpendicular force measurements into the correct direction by using wing position measurements from the potentiometer. These forces were then summed over one flap cycle to determine the average lift. The overall pitch setting of the vehicle was 5º, and the test setup is pictured in Figure 3.1.

Flexible membrane, circular planform wings of 2.5-in span were constructed from carbon fiber rod and balsa wood, with 0.00025-in polyester skin. 1/8-in square balsa wood beams of the same length were set in the shape of an “L” and epoxied together to form the root chord and spar of a planar, circular planform wing. A balsa gusset was added at the corner of the “L” to provide additional strength. Polyester wing planforms were cut into the proper shape and were attached to the wing structure with spray adhesive. A carbon fiber rod of 0.75-in length and 0.05-in diameter extended parallel from the spar, which attached into the mounting arm. The wings were built in four configurations to test nonplanar effects. Nonplanar shapes were created by altering the tip section of a planar wing spar with tip anhedral, a large tip arc, and a small tip arc. These shapes were cut from a sheet of 1/8-in balsa. Only circular planforms were tested to isolate the nonplanar effects. The wing planform and tip shapes are illustrated in Figure 3.2. Each of the five wings was mounted into the test stand at the leading-edge wing attachment point; data was collected at a sampling rate of 15,000 cycles per second over a range of flapping frequencies using a National Instruments data acquisition system. A high sampling rate was selected to ensure good resolution of the force patterns during a single flap cycle, which would result in proper averaging of the forces. A low-grade wind generator was used to simulate a chord-based Reynolds number of approximately 20,000.

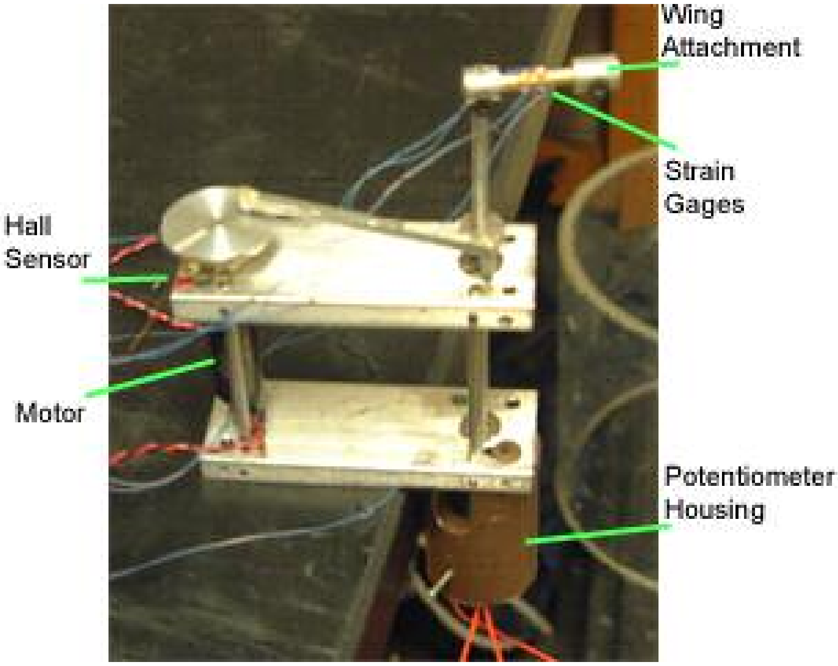

Figure 3.1: Flapping Wing Experimental Test Stand

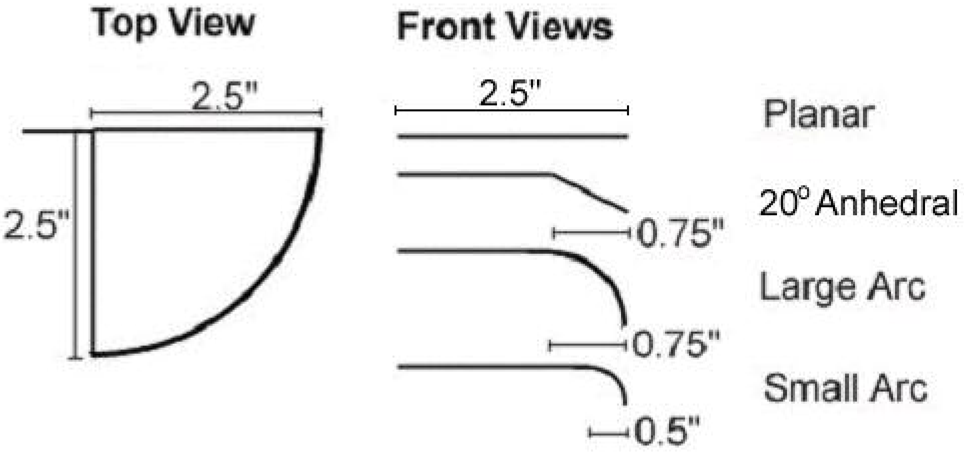

Figure 3.2: Planar and Nonplanar Wing Planforms

3.4.2 Test Stand Results

The results of the test stand experiments are presented in Figures 3.3 and 3.4, for lift and propulsive thrust, respectively. Propulsive thrust is defined as the force exerted by the flapping wing in the direction parallel to the chord line. Lift is defined as the force exerted by the flapping wing in the direction perpendicular to the chord, when the wing is at rest (0° amplitude). The mean values of lift and thrust values were computed over a complete flap cycle, for various flapping frequencies.

The objective of measuring lift was to achieve a total lift of 10 g at 16-18 Hz, and to determine the effect of nonplanar wing tips. Figure 3.3 indicates that the planar wing provides the most lift, with a maximum of 4 g at 10.6 Hz. Although none of the wings reached 10 g of lift, the physical setup of the apparatus did not allow the target frequency range of 16-18 Hz to be tested. Frequencies above 10-12 Hz resulted in very high inertial loads on the wings because of the large moment arm created by the wing attachment part, often resulting in wing failure. However, the upward trend of the data suggests that it may be possible to reach 10 g of lift with the planar, anhedral, or small tip arc wings.

In flapping wing flight, membrane wings reverse camber during the upstroke and downstroke due to inertial and aerodynamic forces, allowing the vehicle to produce an overall net lift. Propulsive thrust is more difficult to generate in membrane wings, so the goal of the propulsive thrust experiments was to ensure that all wings were producing positive amounts of propulsive thrust, and to determine the effect of nonplanar wing tips on propulsive thrust production. Figure 3.4 indicates that the wing with a small tip arc provides the most thrust at higher frequencies. The wing with tip anhedral also provided more thrust than the baseline planar wing at most frequencies.

The overall effect of nonplanar wing tips was beneficial for thrust production and detrimental for lift production. The exception was the large tip arc, which was detrimental to both lift and thrust production. The nonplanar wings may be have experienced losses in lift due to their slightly smaller projected planform area.

The results of this experiment were somewhat disappointing because of the hypothesis that nonplanar wings would reduce negative upstroke lift. However, there were various sources of error in this experiment may have had an effect on the results. The strain gage attachment component increased the moment arm about which the flapping occurred. On the actual MAV, there would be no such moment arm; thus, the resultant velocity and the airflow over the wing would be different and there would be significantly smaller inertial loads imparted on the flapping wings. Additionally, the high inertial loads caused visible torsion in the carbon fiber rod attachment. The freestream velocity was also subject to error due to flow nonuniformity. Due to the sources of error and the mixed results of nonplanar benefit, an in-depth study was undertaken to better understand the underlying physical reasoning of nonplanar effects.

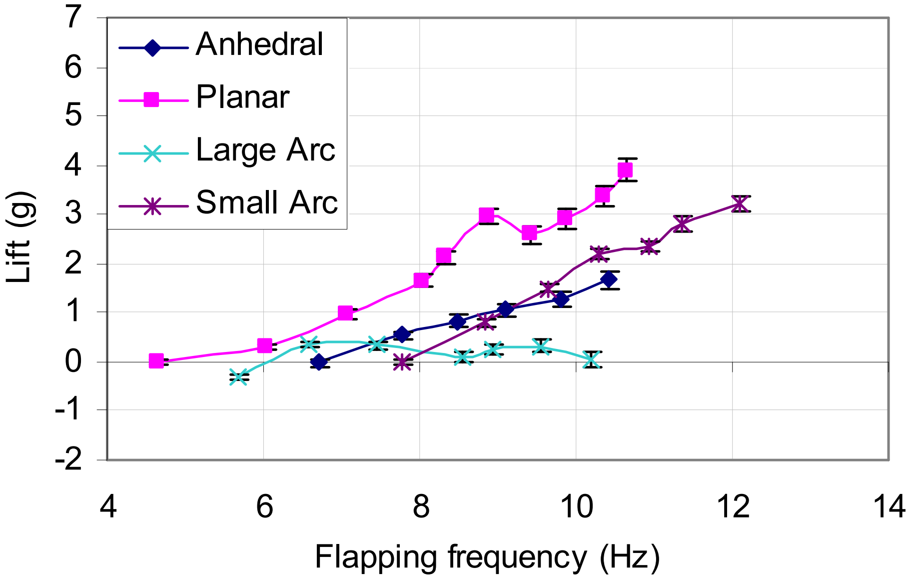

Figure 3.3: Nonplanar Effects on the Lift of Circular Planforms

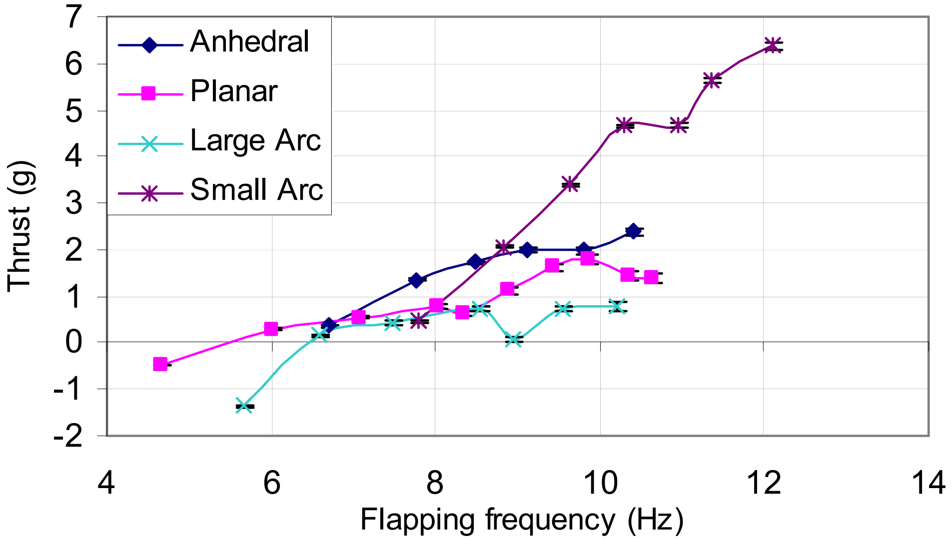

Figure 3.4: Nonplanar Effects on the Propulsive Thrust of Circular Planforms

3.5 MAV Prototype Experiments

The test stand results were unable to reach the flapping frequencies required to produce enough lift for sustainable flight. Therefore, a flapping-wing MAV prototype was developed for additional testing.

3.5.1 Prototype Development

Prototype development began with component selection. The MAV would need a motor, battery, gearbox, receiver, rudder actuator, flexible wing membrane, and strong, lightweight materials for construction of the airframe, flapping mechanism, tail, and wing spars. The MAV components were chosen such that weight of the aircraft would be minimal. The MAV was designated as JLMAV, in reference to Richard Bach's book, Jonathan Livingston Seagull.

3.5.1.1 Propulsion Selection

The propulsion system consists of a motor, battery, and gearbox (if needed). Several small motors were considered in order to choose one to meet JLMAV's needs. The motors considered were: KP00, Didel 4-mm pager motor, and Didel 6-mm pager motor. Table 3-2 shows a comparison of the motor specifications.

Table 3-2: Motor Comparison [59]

Motor	Weight (g)	Dimensions (mm)	Voltage (V)	Resistance (Ω)
KP00	3.5	10 x 8 x 14	3.6	3.6
Didel 4-mm Pager Motor	0.46	4 x 4 x 8	1.2	10
Didel 6-mm Pager Motor	1.5	6 x 6 x 10	0.8	4.5

Generally, the RPM output of a motor is proportional to the voltage input, and—according to the Ohm's Law—the torque of the motor is inversely proportional to the resistance. Since the ornithopter would not be operating at high RPMs, a high voltage was unnecessary. However, in order to drive the flapping mechanism, high torque (low resistance) was desirable. Thus, a 6-mm Didel pager motor was selected for the final configuration because of its low weight and resistance. In order to slow the flapping frequency to 16-18 Hz, a large gear ratio was necessary. The gear ratio was chosen such that the wings would flap at 18 Hz at 70% throttle, when the motor performs most efficiently. A 27:1 gearbox, also manufactured by Didel, would fit the selected motor and meet the flapping frequency requirements. The selected gearbox had two mounting holes for attachment to the airframe. Two 0.05-in carbon fiber rods were inserted into these mounting holes to serve as the main airframe longerons.

In order to supply power to the motor, a battery was required. Electric-powered, remote-controlled (R/C) aircraft currently employ three types of batteries: Nickel-Cadmium, Nickel Metal Hydride, and Lithium Polymer. These types of batteries are compared in Table 3-3. A Lithium Polymer battery was selected for JLMAV because of its high energy density.

Table 3-3: Battery Type Comparison

Battery Type	Capacity	Weight	Advantages
Nickel-Cadmium	Low	High	High discharge rate
Nickel Metal Hydride	Medium	Medium	Environmentally friendly, no memory effect
Lithium Polymer	High	Low	More energy per gram than any other battery

3.5.1.2 Receiver and Actuator Selection

The receiver on an R/C aircraft uses data sent from the transmitter to activate control of the aircraft. The system usually consists of an antenna, servo attachment, battery attachment, any number of servos, and sometimes a speed controller. For JLMAV, the receiver and actuator systems compared were: the Cirrus Micro Joule, HiTec Feather Ultra Micro, RFFS-100, and Plantraco Sub-Micro System. Table 3-4 lists a comparison of these systems.

Table 3-4: Receiver and Actuator Comparison

System	Receiver Weight (g)	Separate Speed Controller?	Number of Channels	Range (m)	Actuator Weight (g)
Cirrus [60]	2.9	Yes (2 g)	4	100	3
HiTec [61]	8	Yes (18 g)	4	300	6.52
RFFS [62]	2.1	No	3	300	1
Plantraco [63]	0.9	No	3	100	1.1

Plantraco's Sub-Micro System was chosen because of its low total weight, and integrated speed controller. The Plantraco system also included a Bohoma 90-mAh Lithium Polymer battery, which attached using innovative magnetic battery terminals—eliminating the need for heavy wire connectors. The Plantraco receiver was mounted between the fuselage longerons, and the battery was mounted such that the center of gravity would be properly positioned. A Plantraco magnetic coil actuator was mounted directly to the empennage to control the rudder. Climbs and descents would be controlled by the throttle.

3.5.1.3 Wing, Tail, and Airframe Construction

All components of the wing, tail, and airframe were constructed with minimum weight in mind. Carbon fiber rods were used for components where the anticipated loads were highest. Balsa wood was used elsewhere. The airframe structure was made of two 0.05-in carbon fiber rods that ran parallel to each other. The wings were constructed of 0.05-in carbon fiber rods, and were hinged along the airframe. One hinge was located just aft of the wing spar, and the other at the aft end of the root rib. The horizontal and vertical tails were composed of balsa wood with 0.000059-in Mylar covering, and the rudder was attached with a Monokote hinge.

3.5.1.4 Flapping Mechanism

A crank-shaft flapping mechanism was chosen for JLMAV. The flapping mechanism was designed such that the weight and asymmetry of the wings would be minimized. The weight was minimized by using a single-crank mechanism, depicted in Figure 3.5. The right and left wing spars are illustrated in bold red and blue, respectively. The illustrated angle is given above each wing spar. Wing hinge points are located just below these numbers, but are not emphasized in the illustration. The conrods were built of 0.05" carbon fiber rod, and utilized cotton thread hinges to connect to the spar and crank arm. A 0.05" steel shaft extended perpendicular to the crank arm, to which the conrods attached. The crank arm itself was built of plastic, and was included with the gearbox.

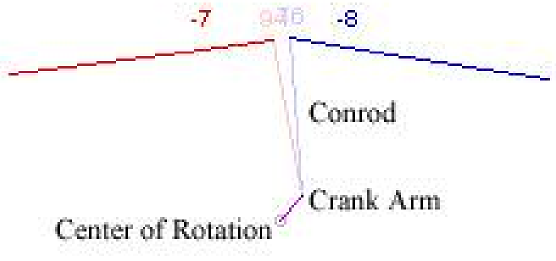

Figure 3.5: Details of Flapping Mechanism [64]

The nature of single-crank flapping mechanisms causes the wings to have an inherent asymmetry—meaning, at each instant in time, the wings are at a slightly different flap angle. The longer the conrod is, the less the asymmetry. The amount of asymmetry for JLMAV is plotted in Figure 3.6.

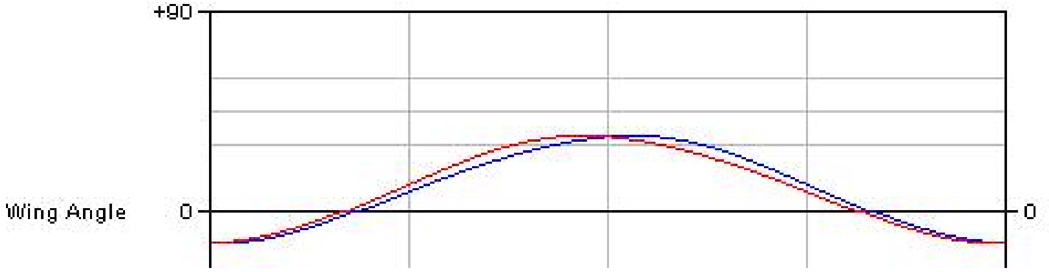

Figure 3.6: Plot of Wing Asymmetry for One Flap Cycle [64]

3.5.2 JLMAV Prototype

The weight of each component is broken down in

Table 3-5, and the JLMAV prototype is pictured in Figure 3.7.

Table 3-5: Weight Statement for JLMAV

Item	Weight (g)	Percent of Total
Motor	1.30	11.9
Airframe (gearbox, structure, wings, tail)	4.27	39.1
Battery	3.18	29.1
Receiver	0.90	8.2
Rudder Actuator	1.20	11.0
TOTAL	10.93	100

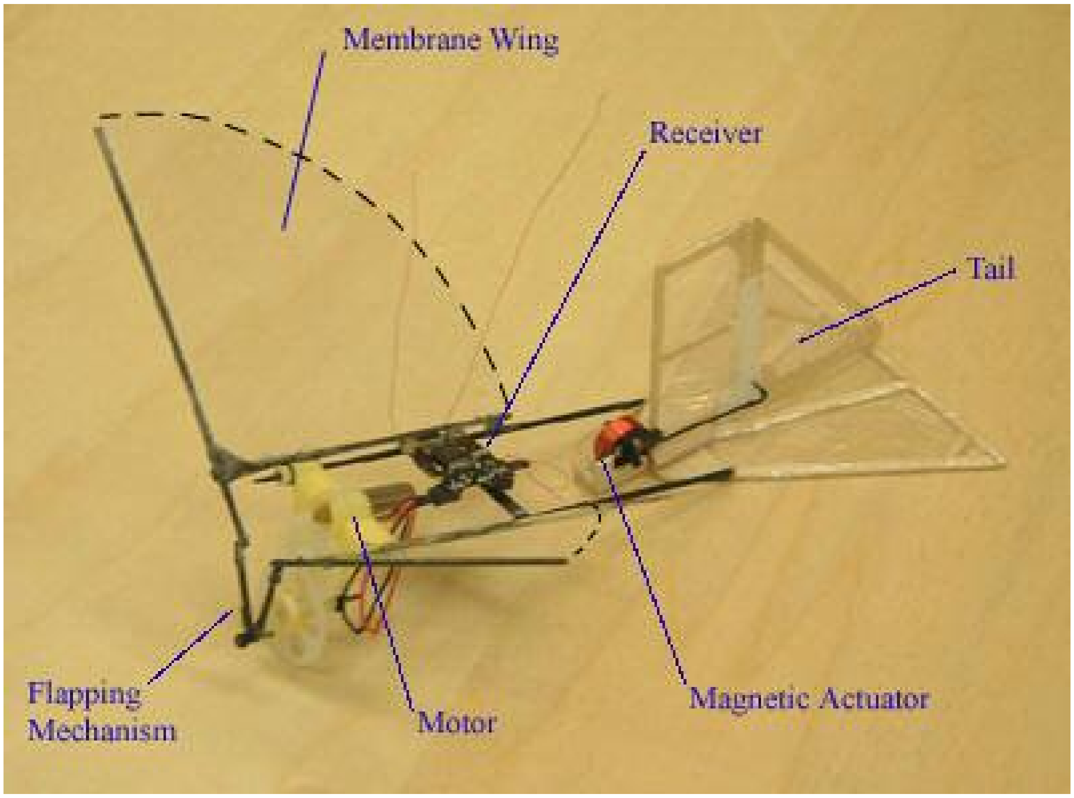

Figure 3.7: Photograph of JLMAV Prototype

3.5.3 Powered Glide Tests

After the construction of JLMAV was complete, indoor powered-glide tests were conducted. Expendable landing gear was attached to protect the gearbox and empennage. The powered-glide tests confirmed that the center of gravity was properly placed, but also suggested that the MAV was not producing enough thrust. During the first test, the throttle was advanced 30%. JLMAV sunk evenly to the ground, indicating proper trim settings. During the second test, the throttle was advanced to 50%. JLMAV demonstrated the same behavior, gliding to the same spot on the floor. At a higher throttle setting, the vehicle should advance farther; thus, it was possible that there was insufficient propulsive thrust.

A simple experiment was conducted to determine if sufficient propulsive thrust was being produced. Suspended from a string in the ceiling, as the throttle is slowly increased, the MAV should begin to fly in a circular pattern under sufficient thrust (see Figure 3.8).

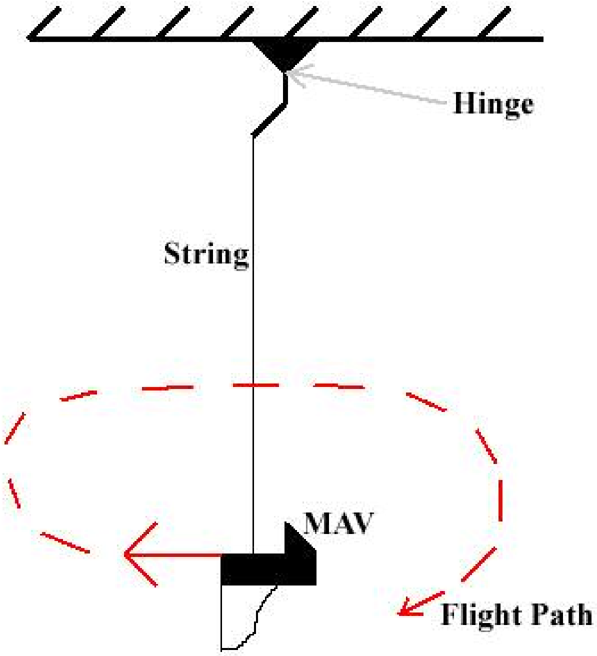

Figure 3.8: Illustration of Qualitative Thrust Test

The test was conducted with the throttle increasing from 0 to 70% (approximately 20 Hz). Inadequate propulsive thrust was produced—perhaps because the polyester membrane wing material was either too heavy or not flexible enough. The wing covering was changed to tissue paper—a common material used for small rubber band-powered ornithopters—and the test was repeated. Though still unsuccessful, the downwash of the wings indicated that the thrust vector from each wing was angled about 45º inward. To correct this problem, a higher aspect ratio wing planform was implemented, and the test was repeated. This time, the MAV flew in a circular pattern—indicating sufficient thrust. The thrust vector was now angled only 10º-15º inward, producing more forward force.

The tests on JLMAV indicated that tissue paper wing skins of a higher aspect ratio improved thrust production, so additional powered glide tests were conducted. These tests were conducted outdoors and uncovered manufacturing and trim issues.

During the first powered glide test, JLMAV made a slow glide to the ground. The tail struck the ground first, and the receiver detached from the airframe. Since the tail struck the ground first, the problem was probably caused by having a far aft center of gravity or too little horizontal tail area. In preparation for the next powered glide test, the receiver was more securely attached and the battery was shifted forward by 1/8 in. Figure 3.9 shows a photograph of this particular test.

Immediately following launch during the second powered glide test, JLMAV made a rapid dive forward and struck the ground nose first. Fortunately, no parts of the vehicle were damaged from the landing. The dive could have been caused by not having enough negative stabilizer, so the horizontal tail incidence was increased.

During the third test flight, JLMAV climbed for approximately 15 ft, then abruptly spiraled to the ground. The vehicle was not damaged during impact. The spiraling tendency was possibly due to a difference between the two wings. Either the wings were flapping at slightly different amplitudes, or one wing membrane had more tension in it than the other. Upon further investigation, it appeared that the wing membranes were no longer uniformly secured, thus the tension needed adjusting. New wing membranes were created and carefully adhered to the vehicle. This test indicated the need for more precise manufacturing techniques to ensure identical performance of the two wings.

Table 3-6: Summary of JLMAV Powered Glide Tests

Test	Wing Material	Summary of Flight
1	Polyester	JLMAV sinks evenly to the floor, indicating a proper center of gravity.
2	Polyester	JLMAV sinks evenly to the floor, possibly insufficient thrust.
1	Tissue	JLMAV strikes the ground tail first, indicating a far aft center of gravity. Battery is shifted forward as a result.
2	Tissue	JLMAV makes a rapid dive, indicating not enough negative stabilizer. Horizontal tail incidence is increased.
3	Tissue	JLMAV climbs momentarily, then spirals to the ground, possibly due to a difference in membrane tension. Wing membranes are reapplied.

Figure 3.9: Powered Glide Test with Tissue Paper Wings

The unsuccessful result of the second round of powered glide tests inspired a wind tunnel investigation to aid in wing selection and trim settings.

3.5.4 Wind Tunnel Test Setup

Since the test stand experiments did not include tissue paper wing skins nor various aspect ratios, JLMAV was converted into a test model for further wing optimization testing. The goal of these tests was to again determine the effects of nonplanar wings, but to also incorporate higher aspect ratio paper skins and a variety of planforms. By using JLMAV as a test model, results were collected at the target flapping frequencies—overcoming major problems with the test stand experiments.

To convert JLMAV into a test model, the battery, receiver, and empennage were removed. The motor was directly connected to a variable power supply. This ensured consistent voltage supply to the motor, whereas the battery lost capacity as it depleted. The empennage and rudder control were unnecessary for wind tunnel testing.

At the center of gravity of the prototype, a 0.05-in carbon fiber rod was mounted vertically using aluminum shim stock and cotton thread hinges. The mounting rod was attached such that it could be loosened to adjust the model for various fuselage angles of attack. At the base of the rod, an aluminum tube was attached that would fit into the openings of a Futek 0.25 lb bending beam force sensor (Figure 3.12). The force sensor was connected to a National Instruments data acquisition system and allowed measurement of the instantaneous lift produced by the vehicle. Data was collected using LabVIEW data processing software.

The test model and mount weighed 5.75 g after modifications. The force sensor was calibrated using incremental weights between 0 and 35 g. A linear distribution was determined, and was applied to the collected data.

The experiments were conducted in the University of Maryland open-jet wind tunnel, which has a 13-in square cross section. The freestream velocity was measured with an Omega HHF92A digital anemometer, which had a resolution of 0.10 kts. Two tissue paper wing planforms were tested: elliptical and polynomial (Figure 3.10). Elliptical planforms are commonly seen on flapping-wing vehicles, but the polynomial shape was chosen because it would maintain a large root chord—where steadier values of lift are produced—yet still allow for a high aspect ratio. Each planform was tested in a planar configuration, with 20º tip anhedral, 20º tip dihedral, and 40º tip anhedral (Figure 3.12). The tip anhedral accounted for 30% of the wing span. Tip anhedral was chosen as the only nonplanar effect to test because of manufacturing simplicity and because it should reduce the wind resistance on the wing during the upstroke, when the wing is producing the largest amounts of negative lift. Each wing was tested at a sampling rate of 5,000 samples per second. Wing planforms were cut simultaneously from the same pattern to minimize construction differences.

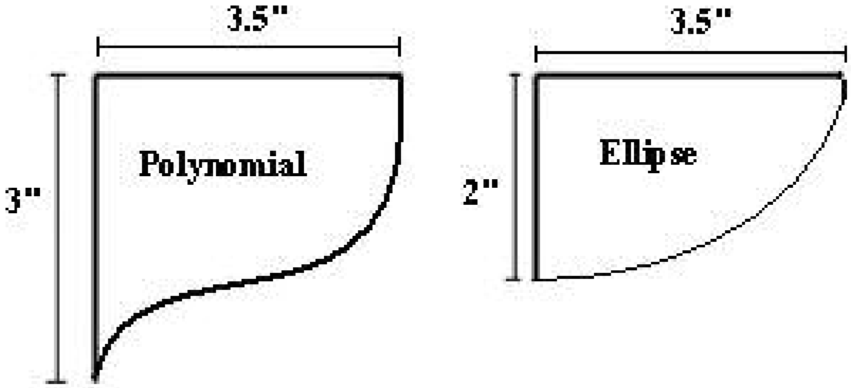

Figure 3.10: Experimental Wing Planforms

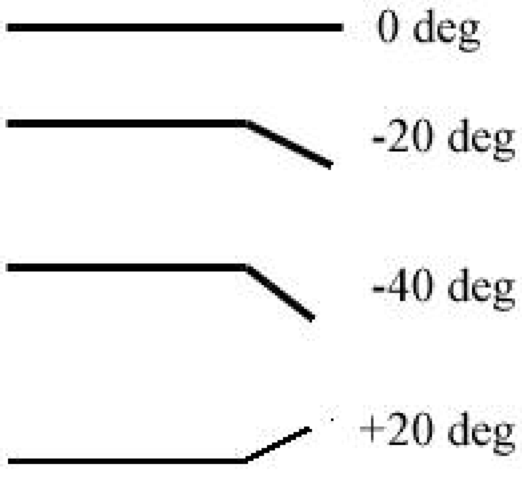

Figure 3.11: Nonplanar Effects (Tip Anhedral and Dihedral)

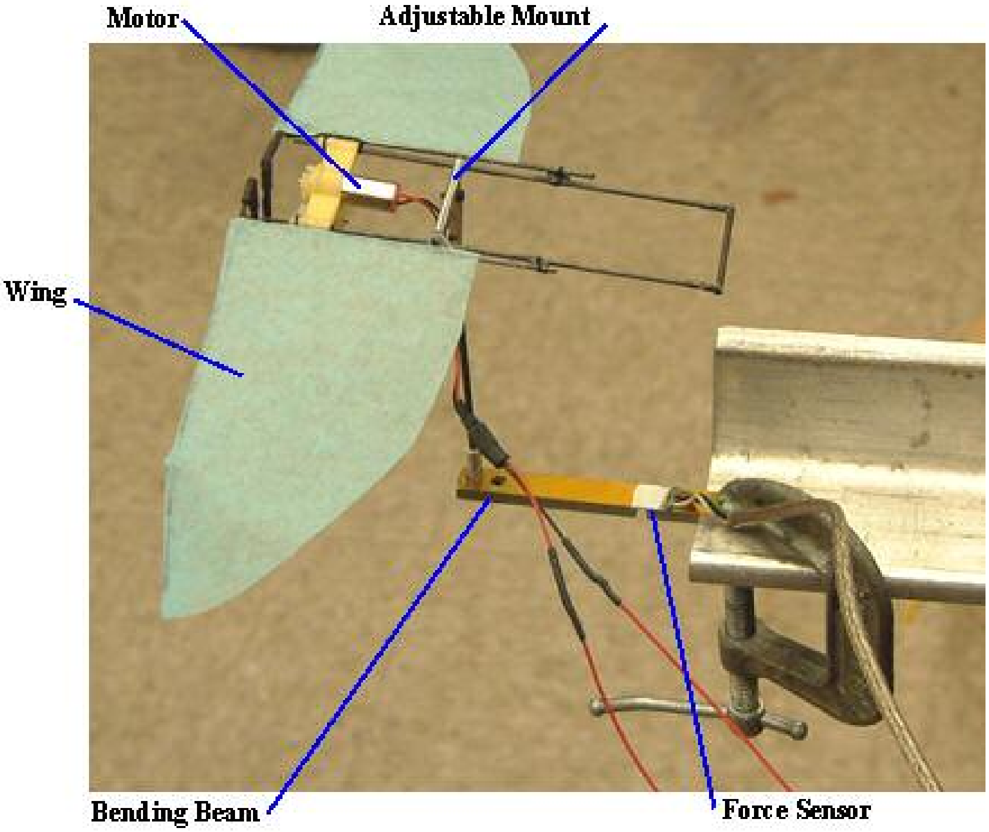

Figure 3.12: JLMAV Test Setup

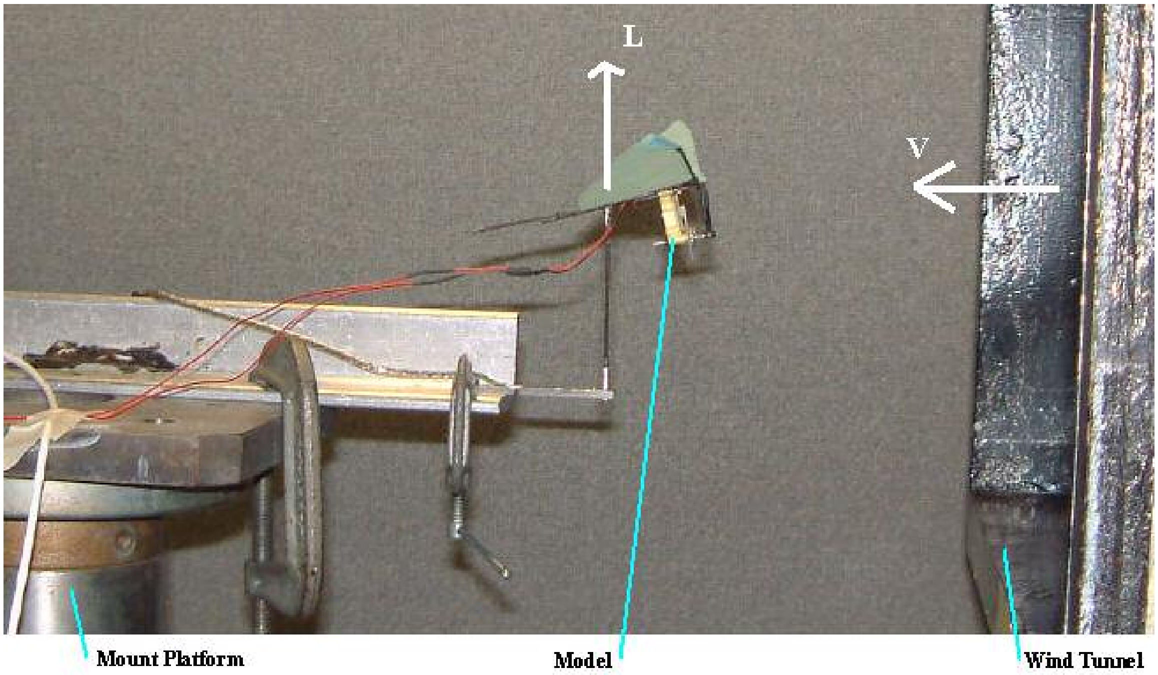

Figure 3.13: Wind Tunnel Test Section Layout

3.5.5 Wind Tunnel Test Results

The lift generated by each planform is plotted for fuselage angles of attack of 6º, 8º, and 10º, where the lift was defined as the net lift over one complete flap cycle. The lift was nondimensionalized according to Equation 3.1, and was plotted versus flapping frequency.

$$C_L = \frac{L}{\frac{1}{2}\rho V^2 S} \qquad (3.1)$$

Where L is the lift, ρ is the air density, V is the freestream velocity, and S is the wing area. The wing area was defined as the projected area of each planform. The projected area of each wing is given in Table 3-7. The reader should be aware of the difference in area and aspect ratio of the two planforms tested when evaluating the results. Each wing was tested at freestream velocities of 5.4 and 8.1 ft/s. These freestream velocities correspond to chord-based Reynolds numbers of approximately 4600 – 9000. The mean chord of the elliptical planform was 1.55 in, whereas the mean chord of the polynomial planform was 1.96 in.

Table 3-7: Projected Planform Areas

Configuration	Elliptical Planform	Polynomial Planform
Planar	13.0 in^2	15.9 in^2
±20˚	12.3 in^2	15.1 in^2
-40˚	10.4 in^2	13.2 in^2

Figure 3.14 shows the lift coefficient variation versus flapping frequency for the elliptical planform at 6º fuselage angle of attack. At a low freestream velocity—indicated by solid lines—the anhedral wings reach higher lift coefficients than their planar counterpart. The 40º anhedral wing reaches the highest lift coefficient, 0.136, and generally creates more lift at high frequencies. In the moderate frequency range, the 20º anhedral wing tends to have higher lift coefficients. At a higher freestream velocity—indicated by dashed lines—the planar and anhedral wings have similar lift characteristics. The dihedral wing generates low lift coefficients at both low and high freestream velocities.

The error bars indicated for the elliptical planform with 20° anhedral at a Reynolds number of 4600 represent the standard deviation of the average lift calculation. The deviation is attributed to the inherent vibration of the vehicle, any flow nonuniformity, signal noise, and other effects. This error is reasonably small and does not affect the overall trend of the data.

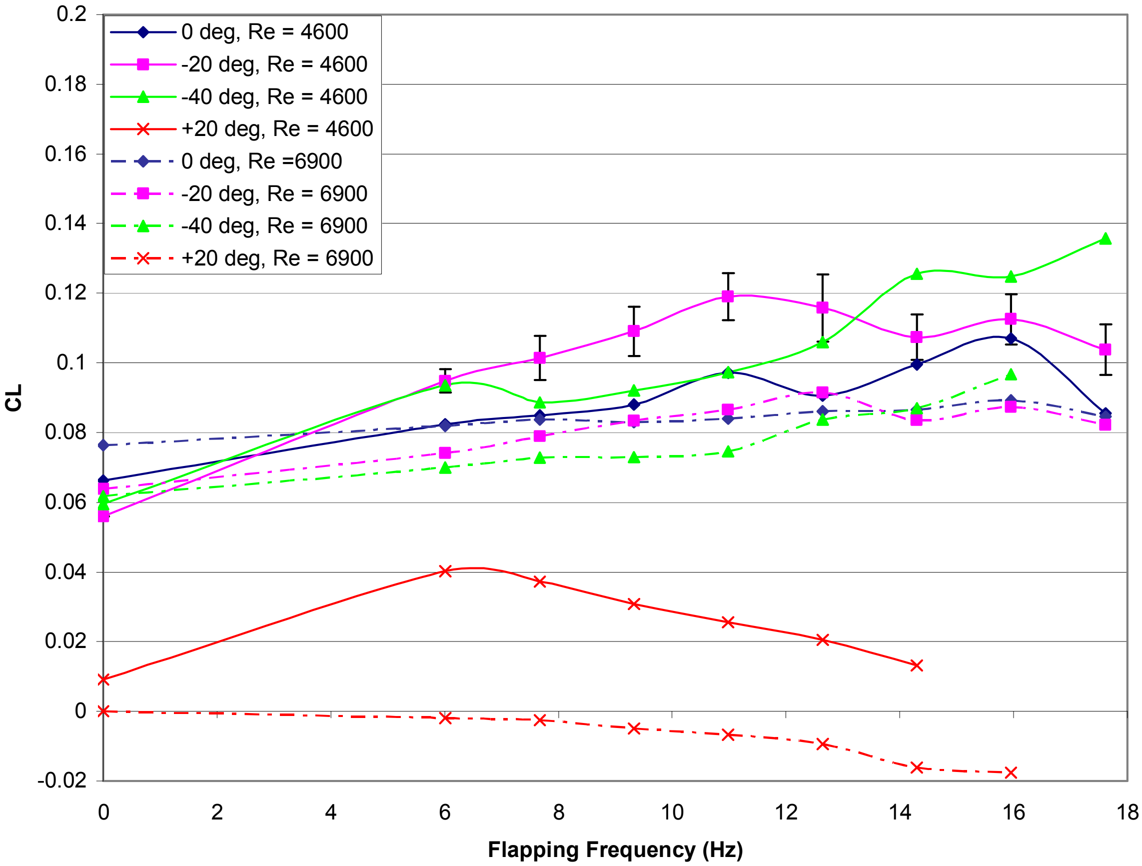

Figure 3.14: Elliptical Planform, $\alpha_f = 6^o$

Figure 3.15 shows the lift coefficient variation versus flapping frequency for the elliptical planform at 8° fuselage angle of attack. At the low freestream velocity, the 20° anhedral wing has slightly better performance than the planar wing, and the 40° anhedral wing has worse performance. At the high freestream velocity, the planar wing performs best, followed by the 20° anhedral wing, then the 40° anhedral wing. The 40° anhedral wing has the same lift coefficient performance for both cases; however, the actual lift produced by the wing was larger at a higher freestream velocity, as expected. This indicates that the Reynolds number may have little effect on lifting capability of the 40° anhedral wing. As in the 6° fuselage angle of attack case, the dihedral wing has poor performance.

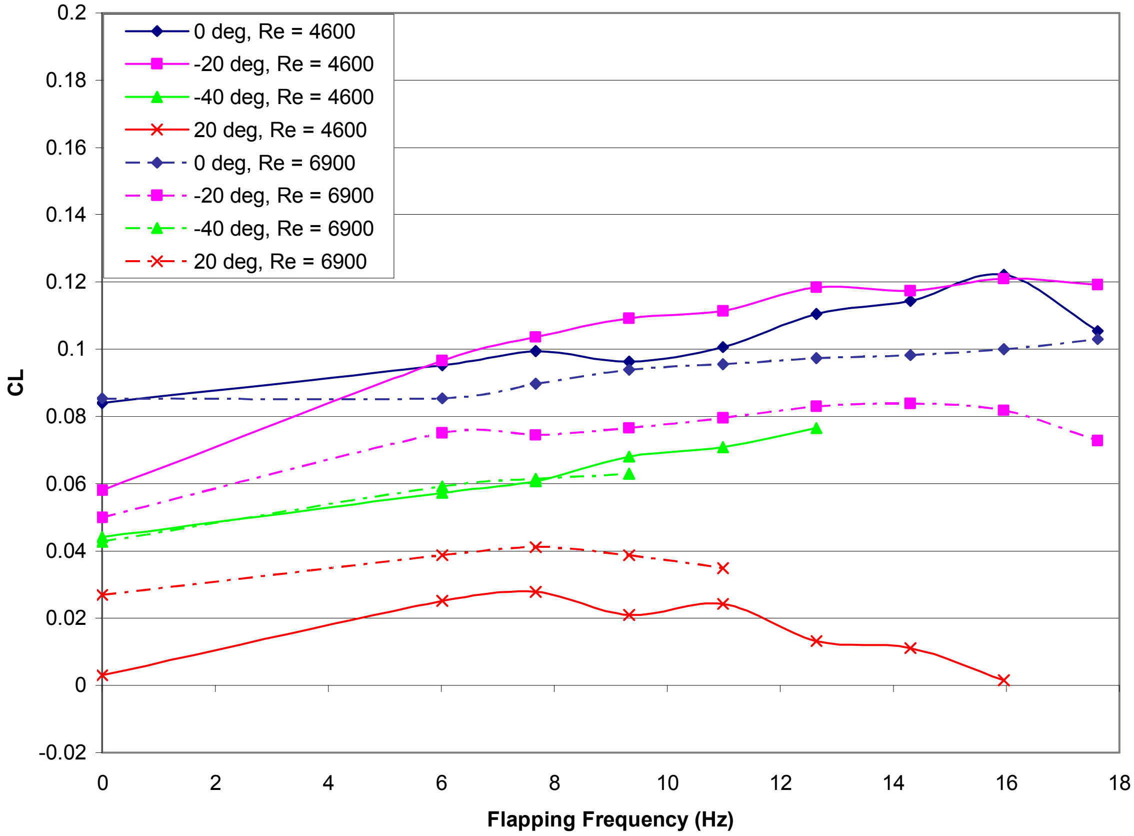

Figure 3.15: Elliptical Planform, $\alpha_f = 8^{\circ}$

Figure 3.16 shows the lift coefficient variation versus flapping frequency for the elliptical planform at 10° fuselage angle of attack. At the low freestream velocity, the planar wing had the best performance, followed by the 20° anhedral wing, and the 40° anhedral wing. The planar wing reached a maximum value of lift coefficient, just above 0.14. At the higher freestream velocity, the planar wing continued to have the best performance, followed by the 40° anhedral wing, then the 20° anhedral wing. As in the 8° fuselage angle of attack case, the 40° anhedral wing had the same performance at both freestream velocities. Additionally, the dihedral wings continued to perform inefficiently.

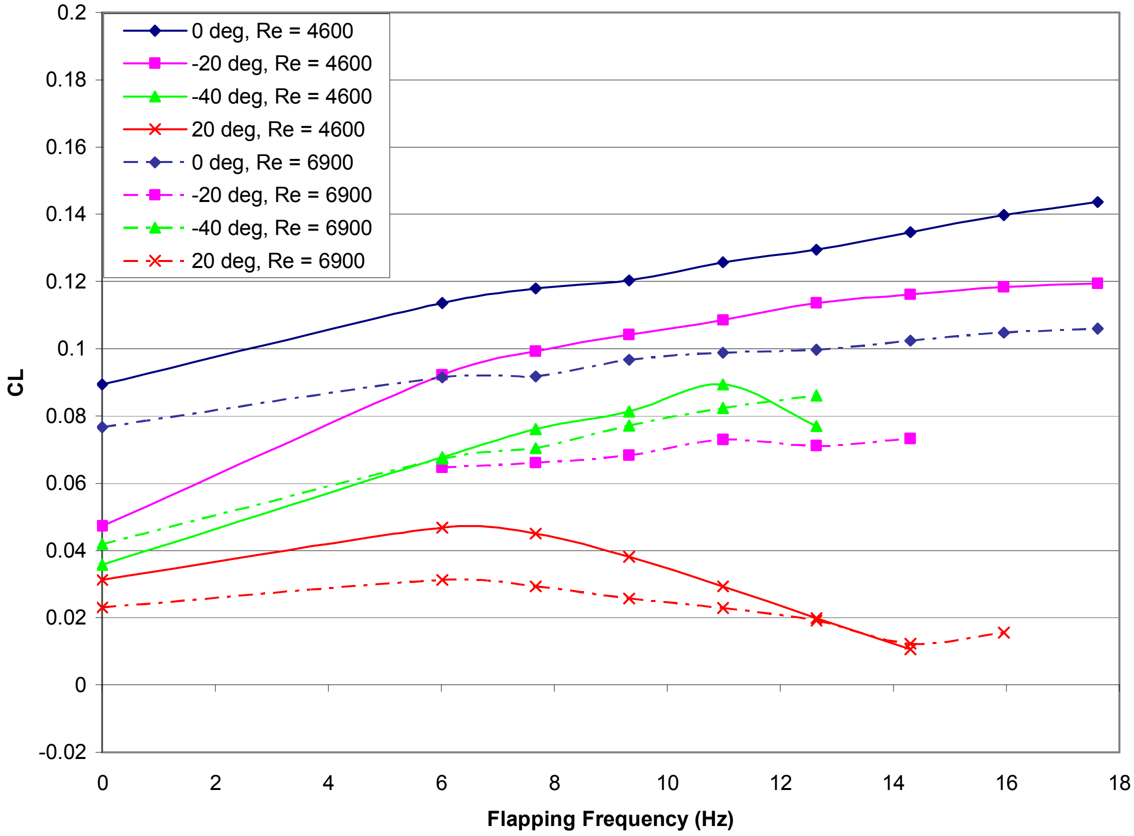

Figure 3.16: Elliptical Planform, $\alpha_f = 10^o$

Overall, the trend of the elliptical planform tends to be that anhedral wings perform better at low fuselage angles of attack, and that planar wings perform better at higher fuselage angles of attack. The results also indicated that the dihedral wings perform poorly in all cases, and that the 40º anhedral wing exhibits an independence from Reynolds number effects.

Figure 3.17 shows the lift coefficient variation versus flapping frequency for the polynomial planform at 6º fuselage angle of attack. At the low freestream velocity, the anhedral wings have significantly better performance than the planar wing. The 40º anhedral wing reaches the highest lift coefficient, just above 0.1. It is followed in performance by the 20º anhedral wing, which reaches a lift coefficient of 0.085. The planar wing has a very flat lift coefficient pattern, with values consistently around 0.027. At the higher freestream velocity, the 40º anhedral wing again has the best performance. It is followed by the planar wing, then the 20º anhedral wing. The dihedral wing continues to generate low lift coefficients.

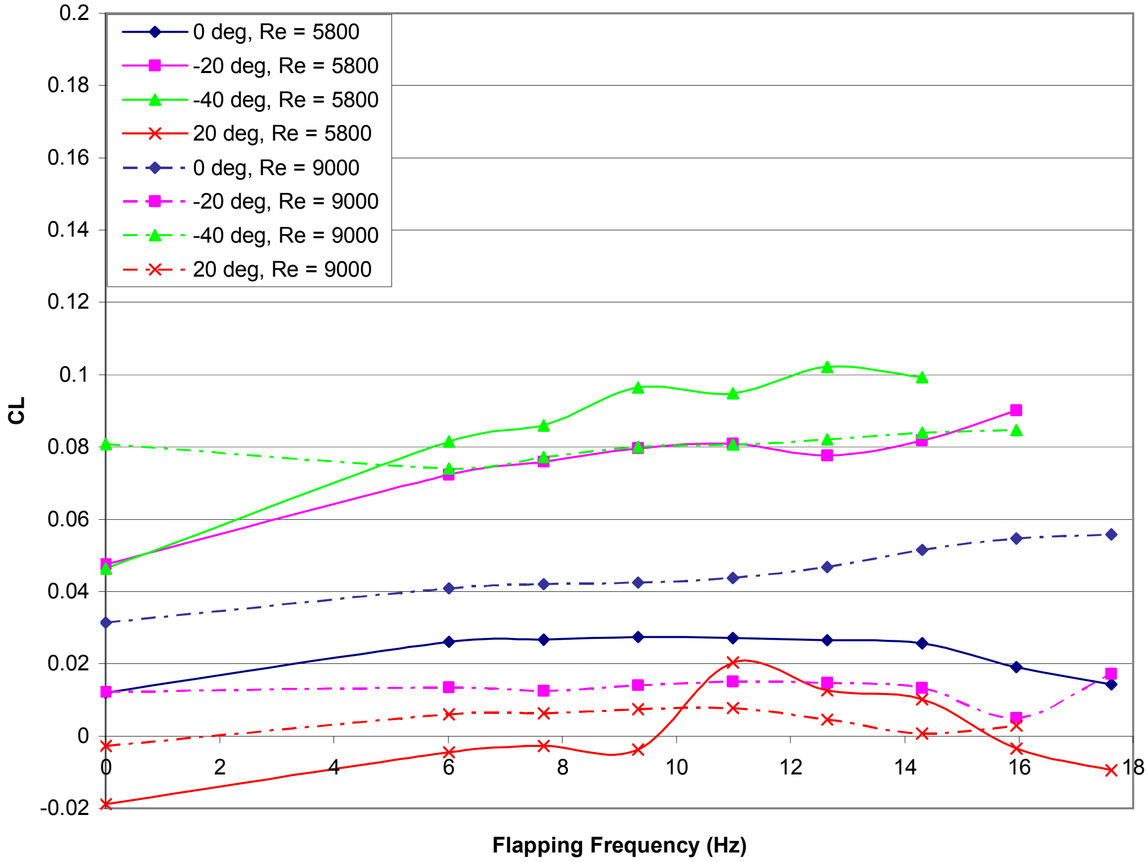

Figure 3.17: Polynomial Planform, $\alpha_f = 6^o$

Figure 3.18 shows the lift coefficient variation versus flapping frequency for the polynomial planform at 8º fuselage angle of attack. At the low freestream velocity, the anhedral wings perform the best and have a similar trend. The 20º anhedral wing reaches the highest lift coefficient of 0.153 at 14.3 Hz. The anhedral wings provide a significant gain over the planar wing, as it reaches a lift coefficient of only 0.072. At a higher freestream velocity, the anhedral wings continue to demonstrate better performance over their planar counterpart. The polynomial planform wings show no indication of Reynolds number independence, as exhibited by the 40º anhedral elliptical planform. All of the polynomial wings have lower lift coefficients at higher Reynolds numbers. Additionally, the dihedral wing continues to perform inefficiently.

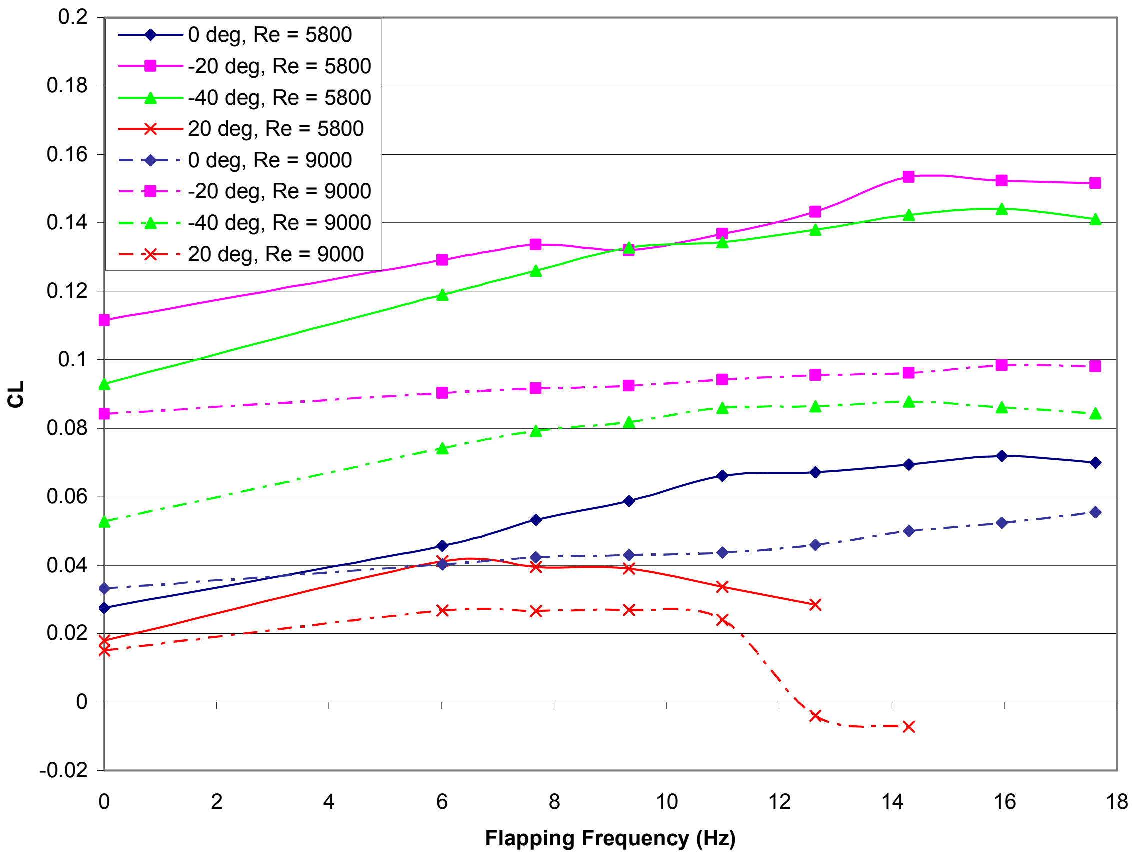

Figure 3.18: Polynomial Planform, $\alpha_f = 8^o$

Figure 3.19 shows the lift coefficient variation versus flapping frequency for the polynomial planform at 10º fuselage angle of attack. At the low freestream velocity, the 20º shows the best performance, reaching the highest lift coefficient overall of 0.18 at 16 Hz. The 40º anhedral wing also reaches high values of lift coefficient, nearing 0.16. The planar wing falls short of these values, reaching a lift coefficient of 0.075. At the higher freestream velocity, the 20º anhedral wing continues to demonstrate the best performance, with lift coefficients approaching 0.12 at 17.8 Hz. This corresponds to an actual value of lift of 15.2 g, the maximum amount of lift generated by any of the wings. The 40º anhedral wing also reaches high lift coefficients, but the planar wing does not perform as favorably.

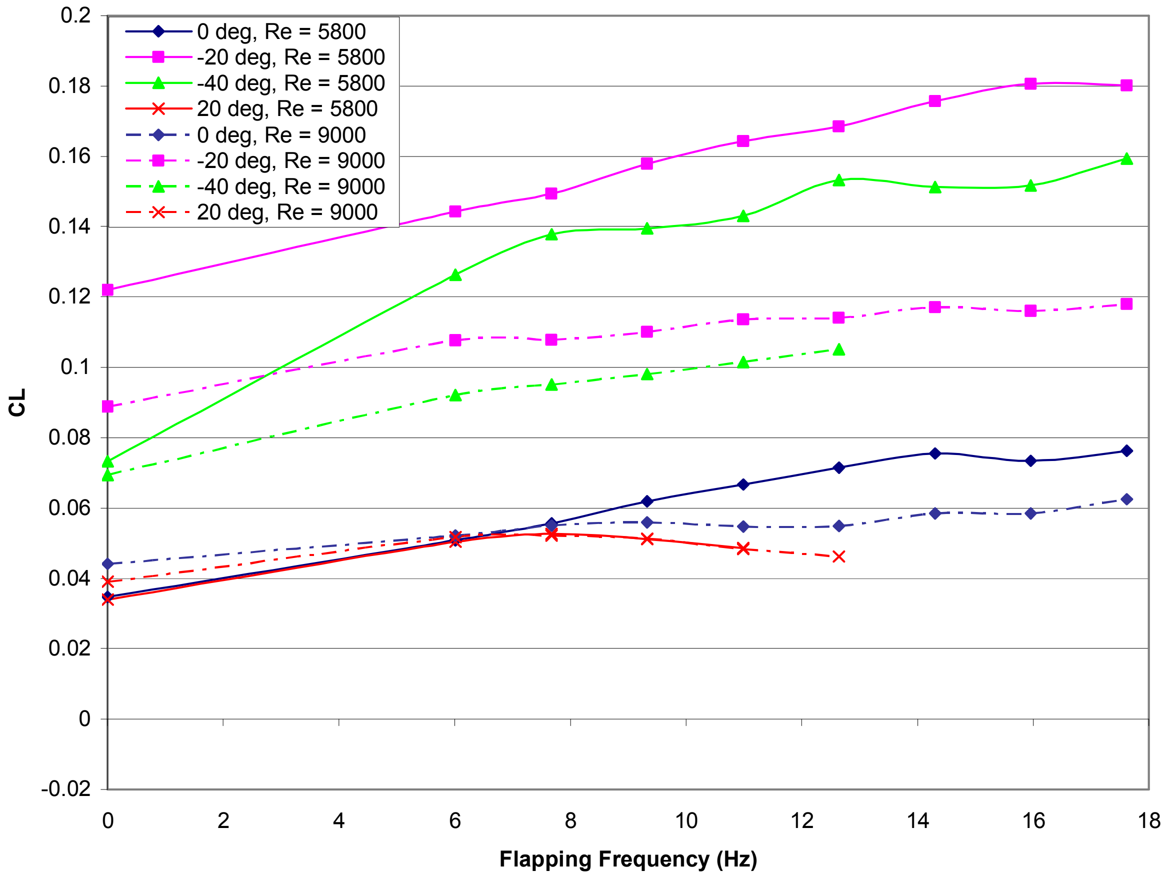

Figure 3.19: Polynomial Planform, $\alpha_f = 10^o$

The polynomial planform results show a consistent benefit of implementing tip anhedral. The 20º anhedral wing reached the highest lift coefficients and the highest maximum value of lift. Unlike in the elliptical planform results, none of the wings demonstrated an independence of Reynolds number. As the Reynolds number was increased, the lift coefficients generally decreased. As expected, the dihedral wing performed poorly.

3.6 JLMAV Wing Selection

Based on the results of these experiments, a specific wing was chosen for JLMAV. The polynomial planform with 20º tip anhedral was selected because of its high lift coefficient trends and total value of lift generated. The wing produced over 15 g of lift at a 10º fuselage angle of attack, more than enough to sustain an 11 g vehicle. The actual values of lift indicate that the vehicle should be trimmed at 8º or 10º fuselage angle of attack, and should be operated at a velocity of around 8 ft/s. At a velocity of 5.4 ft/s, none of the wings were able to generate above 9 g of lift.

Although the polynomial planform was chosen over the elliptical planform, it is important to recall that the two planforms had different wing areas and aspect ratios. The experiment was designed such that the wingspan was fixed, in order to meet the size requirement of MAVs. However, it is difficult to compare the two planforms against each other in a broader sense when the aspect ratio and wing area are not the same.

3.6.1 Thrust Analysis of the Selected Wing

The propulsive thrust generated by the polynomial planform with 20º tip anhedral is plotted for fuselage angles of attack of 6º, 8º, and 10º in Figure 3.20. The propulsive thrust was defined as the net thrust over one complete flap cycle oriented parallel to the freestream velocity. The thrust was nondimensionalized according to Equation 3.2, and was plotted versus flapping frequency.

$$C_T = \frac{T}{\frac{1}{2}\rho V^2 S} \tag{3.2}$$

Where T is the propulsive thrust, ρ is the air density, V is the freestream velocity, and S is the projected wing area. The wing area was defined as the projected area of each planform. Each wing was tested at freestream velocities of 5.4 and 8.1 ft/s. These freestream velocities correspond to chord-based Reynolds numbers of 5800 and 9000, respectively.

The results show highest levels of thrust at 10º fuselage angle of attack, for both Reynolds numbers. At the lower Reynolds number, the wing reaches a peak thrust coefficient of 0.244 at 11 Hz; this corresponds to a thrust value of 13.6 g. The wing produces slightly less thrust as the fuselage angle of attack is decreased to 8º, then to 6º. The thrust tends to peak near flapping frequencies of 11 – 12 Hz for all angles of attack. At the higher Reynolds number, the thrust peaks at a thrust coefficient 0.233 at 6 Hz and 10º fuselage angle of attack, corresponding to a thrust value of 13.0 g. Between 6º and 10º fuselage angle of attack, there is a large decrease in thrust that was not seen at the lower Reynolds number. Additionally, the thrust tends to peak at lower flapping frequencies, between 6 – 10 Hz. Additionally, there is an overall downward trend in thrust production with flapping frequency.

The error bars on the low Reynolds number, 10˚ fuselage angle of attack case represent the standard deviation of the net thrust calculation. The standard deviation is caused by inherent vibration of the wings and other sources, such as flow nonuniformity and signal noise. The standard deviation is reasonably small, and does not affect the overall results.

These results indicate that the wing is able to produce positive levels of thrust, allowing the MAV to sustain a forward flight speed, necessary for high lift production. The wings are more effective for thrust production at lower flapping frequencies, which contradicts the lift trends. The wing reached a maximum value of lift at 17.8 Hz and a high Reynolds number, whereas the thrust peaks at 11 Hz and a low Reynolds number. This suggests that, as the forward flight speed increases, the passive membrane deformations are causing the magnitude and direction of the resultant force to increase and rotate vertically, creating a larger force in the direction of lift and a lesser force in the direction of thrust.

Figure 3.21 shows the instantaneous thrust generated over one flap cycle. The particular cycle depicted is for the case of maximum thrust. The data was collected at a flapping frequency of 11 Hz, freestream velocity of 5.4 ft/s, and a trim setting of 10° fuselage angle of attack—where the wing produced a net thrust of 13.6 g. The instantaneous thrust exhibits a nearly sinusoidal pattern, fluctuating between maximum and minimum values of 37 g and -2 g. The thrust is positive for the majority of the flap cycle, generating negative thrust values only briefly.

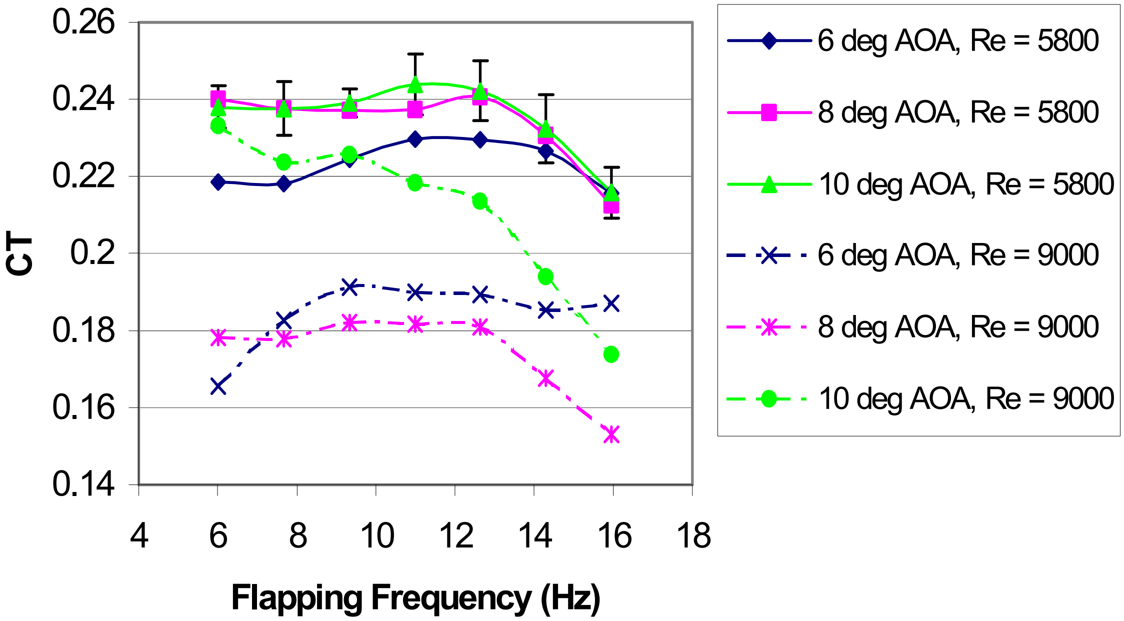

Figure 3.20: Propulsive Thrust of Polynomial Planform with 20º Tip Anhedral

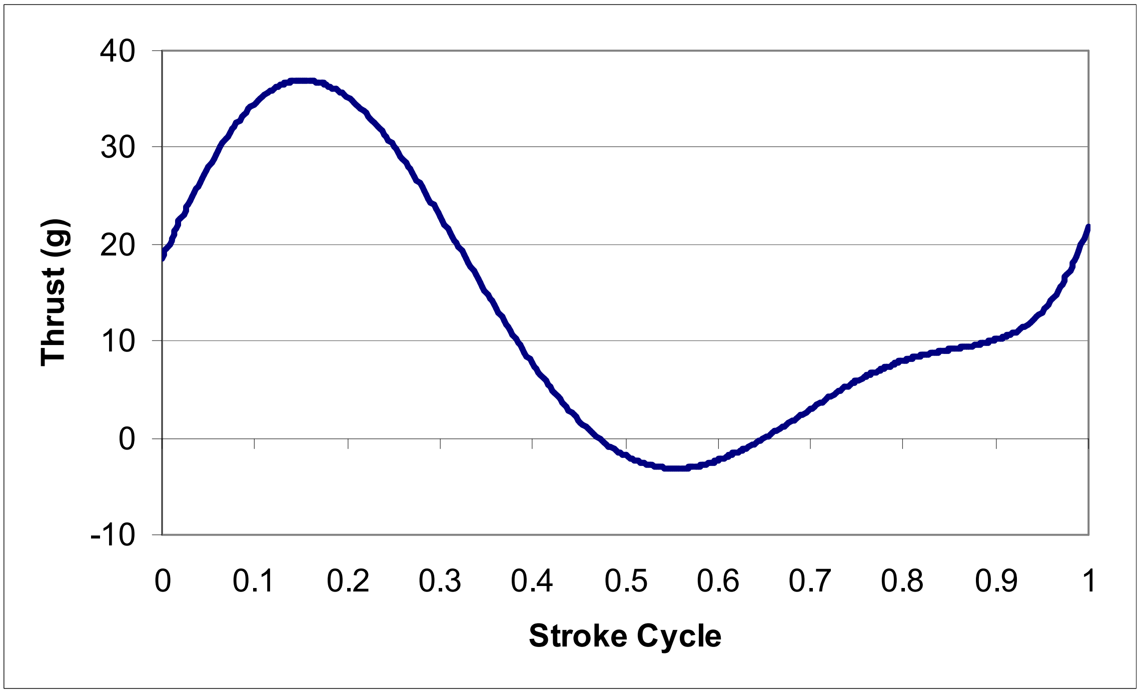

Figure 3.21: Instantaneous Propulsive Thrust of Polynomial Planform with 20° Tip Anhedral at 5.4 ft/s, 11 Hz, 10° α_f

Chapter

4 Explanation of Results

4.1 Instantaneous Lift

By looking at the instantaneous lift produced over a single flap cycle, some insight is gained into why the nonplanar planforms perform better than their planar counterparts. Since the polynomial planform with 20º tip anhedral was selected for JLMAV, it was examined in detail. In Figure 4.1, the instantaneous lift of a planar and nonplanar polynomial planform wing at 10º fuselage angle of attack is plotted for a single wingstroke cycle at approximately 16 Hz and a freestream velocity of 8.1 ft/s.

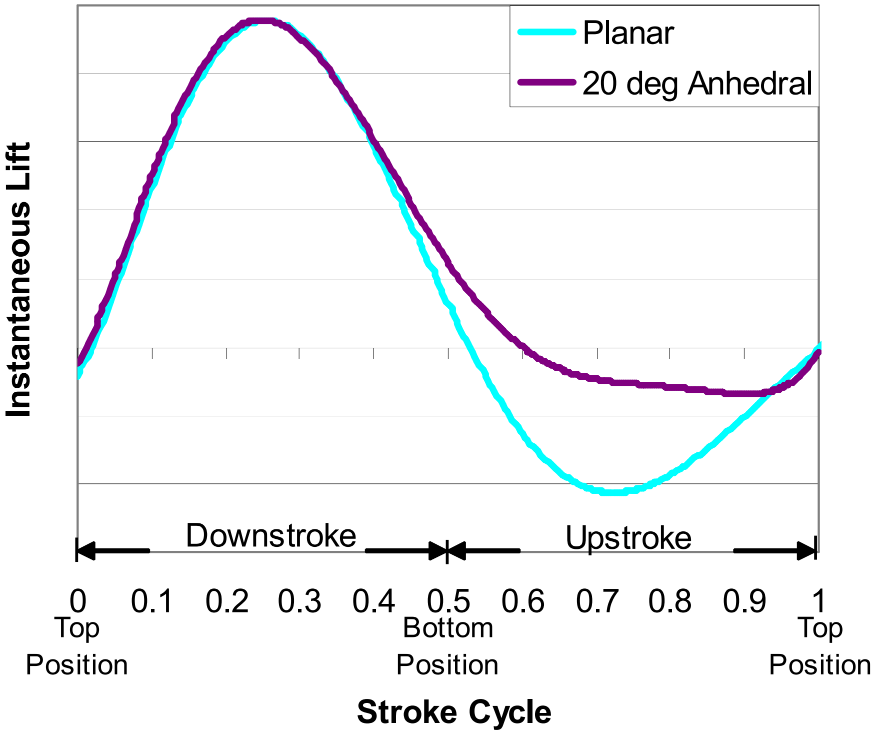

Figure 4.1: Instantaneous Lift Produced by Planar and Anhedral Polynomial Membrane Wings

The plot of instantaneous lift shows that the downstroke of the planar and 20° tip anhedral wings are very similar. There is little difference between the total amount of lift generated. By taking the integral of the curve on the downstroke, the planar and nonplanar wings differ in area by only 4.5%.

The upstroke is where the nonplanar wing makes a significant difference. The nonplanar wing produces significantly less negative lift on the upstroke. To quantify the difference in negative upstroke lift, the integral of the curves was calculated over the upstroke. The planar wing produces 4.3 times more negative lift than the nonplanar wing. This proves that the nonplanar tips do reduce negative lift on the upstroke, as hypothesized.

The instantaneous lift can also be used to show why the dihedral wing performed so poorly. In Figure 4.2, the planar polynomial wing is compared to the 20° dihedral wing. Both wings are compared at 10° fuselage angle of attack, 16 Hz flapping frequency, and a freestream velocity of 8.1 ft/s. The instantaneous lift is plotted for a single wingstroke cycle. The figure indicates that the dihedral wing reaches a higher maximum value of both positive and negative lift. During the downstroke, the additional lift might be attributed to circulation around the tip region; however, this lift quickly dissolves as the upstroke begins. A large amount of negative lift characterizes the upstroke, presumably due to increased drag caused by the dihedral tips. However, near the end of the upstroke, the dihedral wing begins to produce positive upstroke lift. This could be caused by a buildup of circulation over the wing. Nevertheless, the dihedral wing is still less effective overall because of the large amount of negative lift over a larger portion of the upstroke.

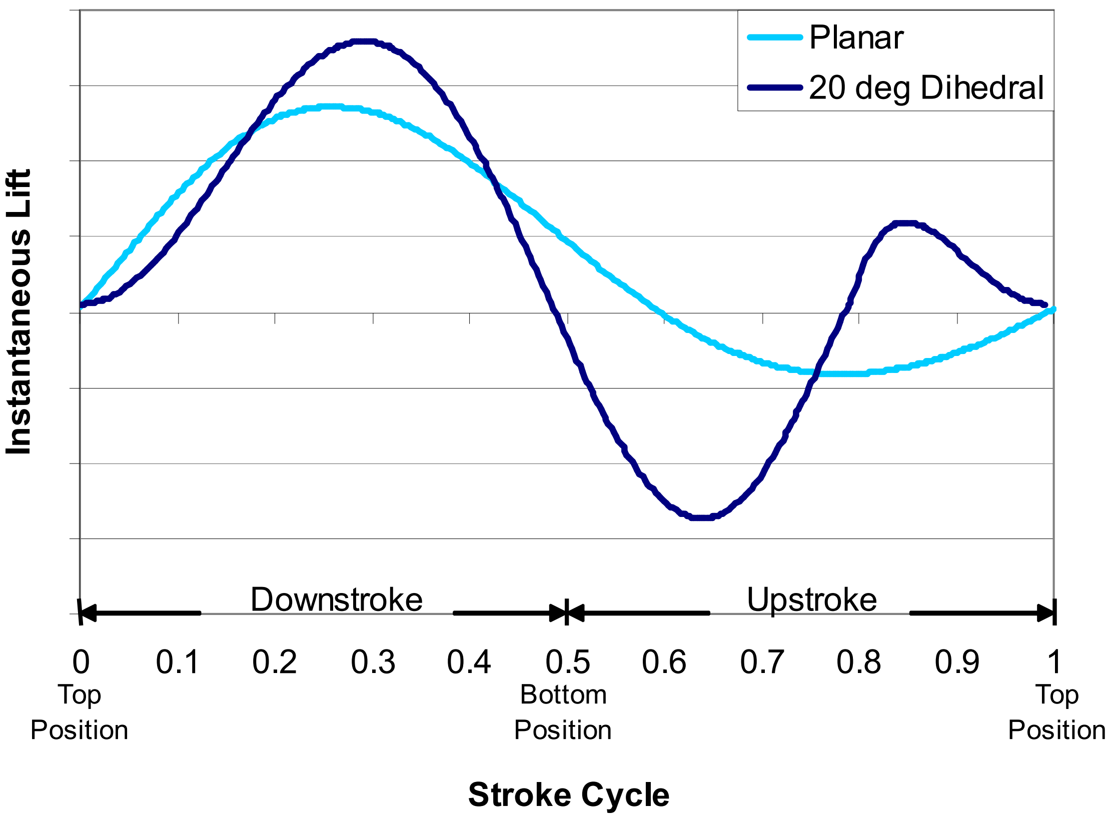

Figure 4.2: Instantaneous Lift Produced by Planar and Dihedral Polynomial Membrane Wings

4.2 Strobe Analysis

In order to visualize how the flexible membrane was deforming on the preferred wing, a strobe analysis was done. The polynomial wing with 20º tip anhedral was attached to the vehicle, and the vehicle was clamped in a vise. A strobe light with variable flash rates was positioned next to the opening of the open-jet wind tunnel. The freestream velocity of the wind tunnel was set at 8.1 ft/s. The strobe and flapping frequency of the wings were synchronized at approximately 11 Hz, creating a nearly still image of the wings at various points in the flap cycle. Photographs and video were taken from various viewing angles. The vibration of the model caused some blur in the photographs, but the deformation of the wings is still visible.

In Figure 4.3, the polynomial wing with 20º tip anhedral was positioned at the top of the downstroke. The spar is accentuated in lime green; the trailing edge is accentuated with a red dashed line. The membrane appears to take a concave form, providing positive camber. Figure 4.4 shows the wing as it sweeps through the downstroke. The positive camber continues, and the position of the trailing edge indicates a “parachute effect,” allowing the wing to produce larger amounts of lift.

In Figure 4.5, the wing is at its bottom position. Here is where the reduction in negative upstroke lift becomes apparent. In (a), the trailing edge appears to dip down considerably over a large portion of the span, which would reduce the drag on the upstroke. This dip is confirmed through a side view (b). To truly see how tip anhedral affects this part of the flap cycle, strobe photographs were also taken of the planar wing. A side view of the planar wing is shown in Figure 4.6. It indicates that the trailing edge cannot reduce its profile as much as the anhedral wing on the upstroke.

The deformation of the trailing edge of the anhedral wing continues during the upstroke, as indicated in Figure 4.7. This photograph also shows a downwash at the tip during the upstroke, which could be contributing to propulsive thrust generation.

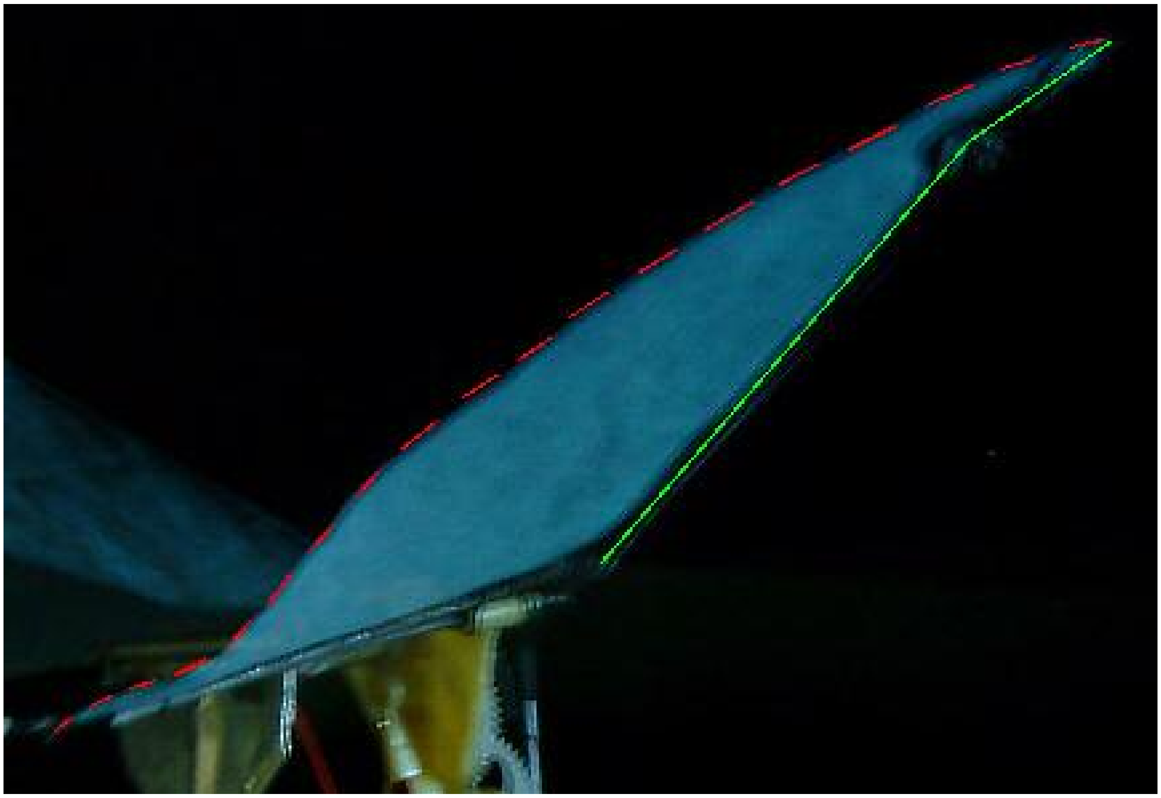

Figure 4.3: Anhedral Strobe Results - Top of Downstroke

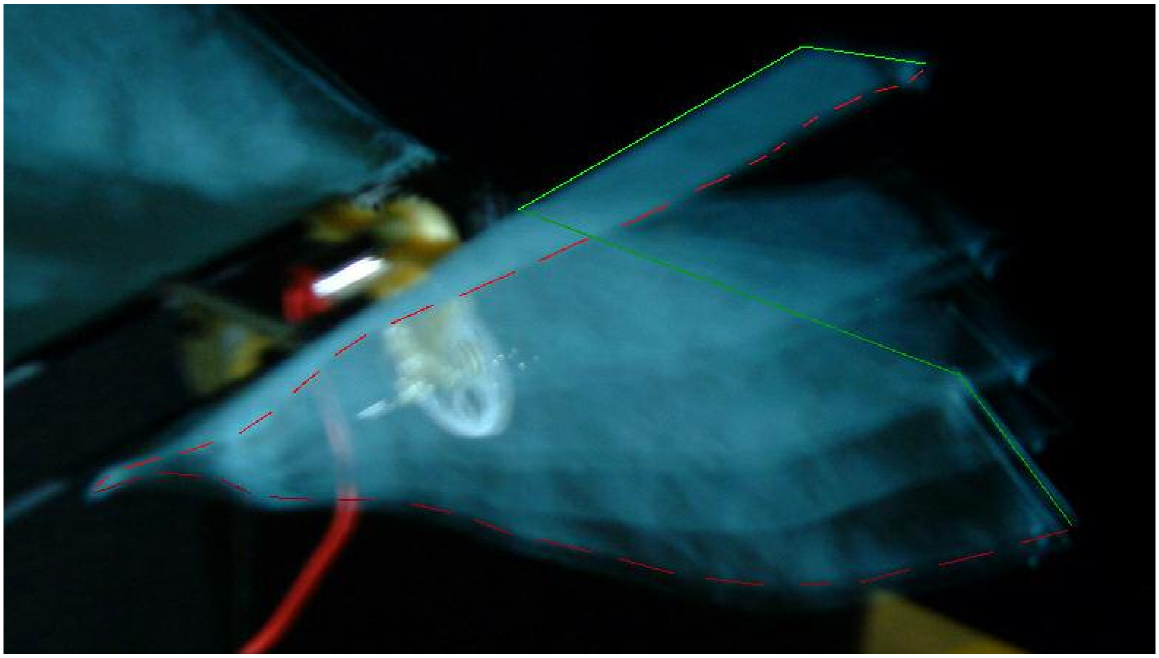

Figure 4.4: Anhedral Strobe Results - The Downstroke

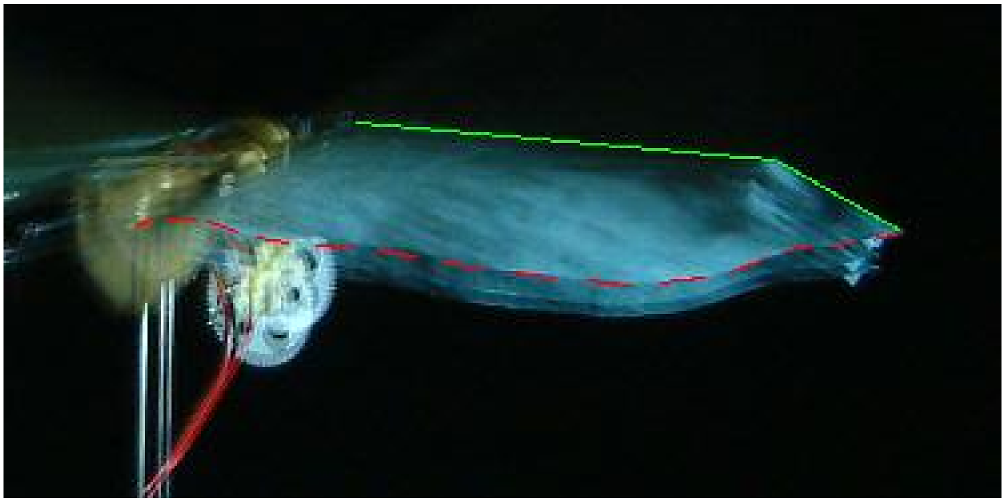

(a) Rear View of Bottom Position

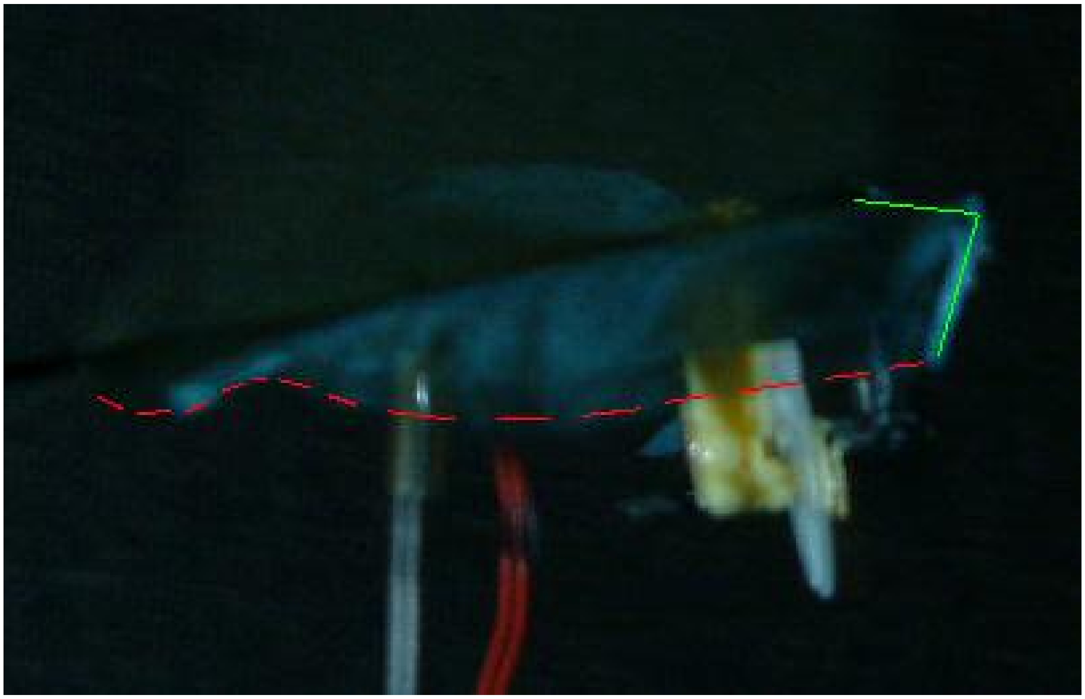

(b) Side View of Bottom Position

Figure 4.5: Strobe Results - Bottom Position

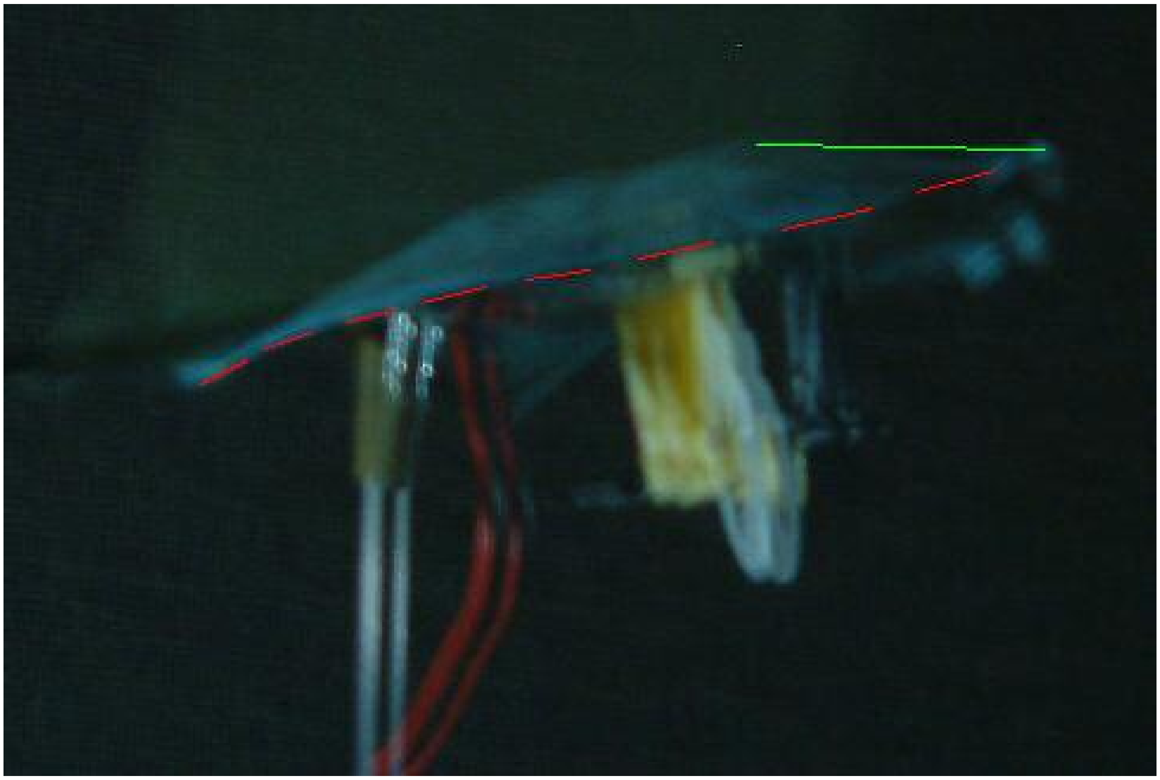

Figure 4.6: Planar Strobe Results - Side View at Bottom Position

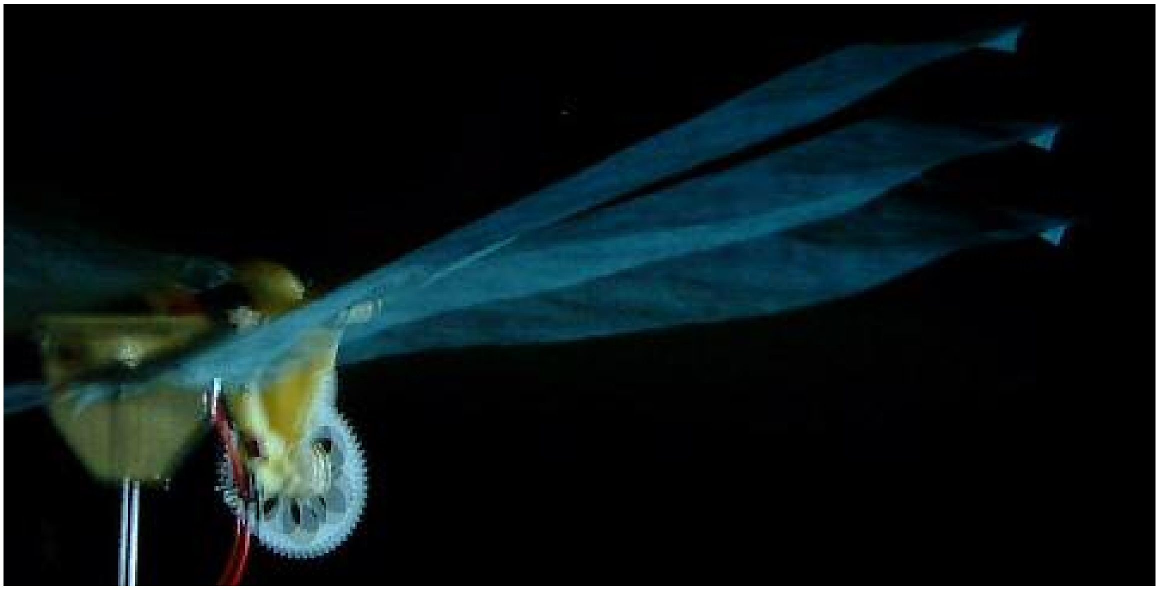

Figure 4.7: Anhedral Strobe Results - The Upstroke

Chapter

5 Conclusions and Future Work

5.1 Summary and Conclusions

Test stand experiments were conducted to measure the lift and propulsive thrust generated by circular planform, membrane flapping wings with a variety of nonplanar tips. The nonplanar tips investigated were: tip anhedral, large tip arc, small tip arc, and planar tip. Forces were collected over a range of flapping frequencies. As the flapping frequency was increased, the lift and propulsive thrust tended to increase for most of the wings tested. These initial experiments indicated that nonplanar wings were generally beneficial to thrust production but detrimental to lift production in circular planform, flapping wings. Wings with tip anhedral or a small tip arc were able to produce more propulsive thrust than their planar counterpart; however, the planar wing produced up to 2 g more lift than the nonplanar wings at higher frequencies. The test stand experiments were unable to reach the required flapping frequencies because of high inertial loads, so a prototype model was designed and built for more accurate experiments.

The prototype model was tested in an open jet wind tunnel at two freestream velocities. Elliptical and polynomial wing planforms were tested in a planar, 20º tip anhedral, 40º tip anhedral, and 20º tip dihedral configuration. The wings were tested for fuselage angles of attack of 6º, 8º, and 10º. Lift values were collected over a range of flapping frequencies. As flapping frequency increased, the lift generally tended to increase. As velocity and fuselage angle of attack were increased, the wings also produced more lift. Results indicated that nonplanar wings were beneficial to lift production for the polynomial planform. For all fuselage angles of attack tested, the anhedral wings consistently performed better than the planar polynomial wing. The polynomial planform with 20º tip anhedral produced the most lift overall, reaching a maximum value of 15.2 g at 17.8 Hz and 10º fuselage angle of attack. Nonplanar wings were beneficial on elliptical planforms only at low fuselage angles of attack. At 6º fuselage angle of attack, both the 20º and 40º anhedral tips performed the same or slightly better than the planar wing at a low Reynolds number; at a higher Reynolds number, the planar and anhedral wings had similar performance. At 8º fuselage angle of attack, only the 20º anhedral wing continued to perform better than the planar wing at a low Reynolds number. At 10º fuselage angle of attack, the planar elliptical wing performed better than both anhedral wings at both Reynolds numbers tested. For all cases, the dihedral wing performed poorly.

Based on the wind tunnel results, the optimum wing configuration for a flapping-wing MAV was determined to be a polynomial planform with 20º tip anhedral, trimmed at 10º fuselage angle of attack. A thrust analysis of the selected wing indicated that positive levels of thrust were generated at all angles of attack and wind speeds, although the thrust tended to decrease at high wind speeds and high flapping frequencies.

An instantaneous lift analysis indicated that tip anhedral was reducing negative upstroke lift, as hypothesized. The selected wing had similar downstroke characteristics as its planar counterpart. However, the negative upstroke lift of the planar wing was 4.3 times greater than that of the 20º tip anhedral wing, giving the anhedral wing a significant advantage. Strobe photography indicated that the benefit of tip anhedral on membrane flapping wings was largely due to its ability to twist farther downward on the upstroke, which reduced the profile drag experienced by the wing.

5.2 Recommendations for Future Work

There are many opportunities for future work on JLMAV. An immediate follow-on to this research might be a more detailed thrust comparison of the nonplanar planforms tested herein (not just the selected wing).

The prototype vehicle could be converted into a flying vehicle, such that systematic flight tests could verify the effects of nonplanar tips. The challenge of flight testing lies in repeatable manufacturing techniques and incorporating a small measuring unit to record data.

Another option for future work on JLMAV would be to perform detailed flow visualization techniques, which would provide a better understanding of the flow characteristics surrounding membrane wings. This would be especially helpful for quantifying the effects of nonplanar tips. Ideally, flow visualization tests would be performed in “hover” conditions and in the wind tunnel. Then the “hover” effects could be isolated from aerodynamic phenomena caused by a freestream velocity.

A detailed CFD analysis would be useful for future work on JLMAV. A membrane, flapping wing model adaptable for nonplanar wings could allow nonplanar effects to be optimized to their fullest extent.

Another option would be to explore easily repeatable manufacturing techniques relevant to flapping membrane wing construction. These techniques would minimize the obstacles encountered during flight testing due to trim issues or asymmetric membranes. A feedback control system could also be implemented into the vehicle to improve stability. This stability augmentation system would allow the MAV fly in more demanding environments, and it could minimize the pilot's workload. Such a system might also be able to provide vehicle navigation, if carefully designed.

Another option would be to explore other means of decreasing the negative upstroke lift of membrane wings. This could be accomplished by testing fully nonplanar wings, which might include concepts like the hyper-elliptical cambered span (HECS) wing (Figure 5.1). Reducing negative upstroke lift might also be achieved by incorporating active wing morphing or composite aeroelastic tailoring. An active wing concept might implement anhedral on the upstroke and dihedral on the downstroke. This would be an interesting concept to test since the instantaneous lift results herein showed an increase in lift on the downstroke caused by the 20˚ dihedral wing, and a reduction in negative upstroke lift caused by the 20˚ anhedral wing.

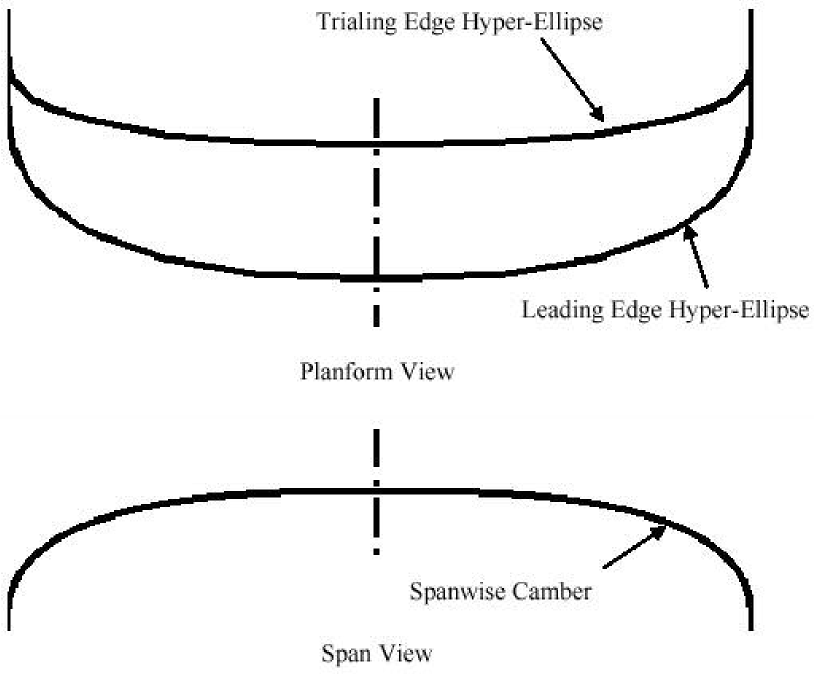

Figure 5.1: Illustration of HECS Wing [65]

BIBLIOGRAPHY

[1] McMichael, J., and Francis, M., "Micro Air Vehicles – Toward a New Dimension in Flight," http://euler.aero.iitb.ac.in/docs/MAV/www.darpa.mil/tto/MAV/mav_auvsi.html, August 1997.

[2] Vogel, S., Life in Moving Fluids, 2nd ed., Princeton University Press, Princeton, NJ, 1994.

[3]Tousley, B., "Micro Air Vehicle Advanced Concept Technology Demonstration," http://www.darpa.mil/ucar/programs/mav.htm, March 2006.

[4] Alexander, D.E., Nature's Flyers, Johns Hopkins University Press, Baltimore, 2002.

[5] Mueller, T., and DeLaurier, J., "An Overview of Micro Air Vehicle Aerodynamics," Fixed and Flapping Wing Aerodynamics for Micro Air Vehicle Applications, Vol 195, Progress in Astronautics and Aeronautics, AIAA, 2001.

[6] Bohorquez, F., and Pines, D., "Rotor and Airfoil Design for Efficient Rotary Wing Micro Air Vehicles," *61st Annual American Helicopter Society Forum*, Grapevine, TX, June 2005.

[7] Hein, B., and Chopra, I., "Hover Performance of Micro Air Vehicles: Rotors at Low Re," *American Helicopter Society International Speicalists' Meeting on Unmanned Rotorcraft*, Chandler, AZ, January 2005.

---

[8] Falcon Models, http://www.falconmodels.uk.com/index.html, Location: United Kingdom.

[9] Plantraco Hobbies, http://www.plantraco.com/hobbies/, Location: Saskatoon, SK, Canada.

[10] "Procerus Technologies: Kestrel Autopilot," http://www.procerusuav.com/productsKestrelAutopilot.php, Location: Vineyard, UT.

[11] Conroy, J., Samuel, P., and Pines, D., "The Evaluation of Optic Flow Data Using a Wireless Telemetry System for Micro Air Vehicle Applications," *American Helicopter Society International Specialists' Meeting on Unmanned Rotorcraft*, Chandler, AZ, January 2005.

[12] Stuerzl, W., and Srinivasan, M., "Omnidirectional Vision with Frontal Stereo," *Proceeding of 27th Annual Meeting of the German Association for Pattern Recognition*, 2005.

[13] Barrows, G.L., Neely, C., and Miller, K.T., "Optic Flow Sensors for MAV Navigation," Fixed and Flapping Wing Aerodynamics for Micro Air Vehicle Applications, Vol 195, Progress in Astronautics and Aeronautics, AIAA, 2001.

[14] Cesar, A., "Integrated Energy Supply and Wing Structure for Micro Air Vehicles," http://www.darpa.mil/DSO/thrust/matdev/smfm/lynntech.html, Arlington, VA.

[15] Cowley, M., "AeroVironment's 'WASP' Micro Air Vehicle Sets World Record," http://www.aerovironment.cn/news/news-archive/wasp62.html, Simi Valley, CA.

[16] Thom, A., and Swart, P., “The Forces on an Aerofoil at Very Low Speeds,” *Journal of the Royal Aeronautical Society*, Vol. 44, 1940, pp. 761-770.

[17] Kunz, P.J., and Kroo, I., “Analysis and Design of Airfoils for Use at Ultra-Low Reynolds Numbers,” Fixed and Flapping Wing Aerodynamics for Micro Air Vehicle Applications, Vol 195, Progress in Astronautics and Aeronautics, AIAA, 2001.

[18] Laitone, E.V., “Wind Tunnel Tests of Wings at Reynolds Numbers Below 70,000,” *Experiments in Fluids*, Vol. 23, 1997, pp. 405-409.

[19] Torres, G.E., and Mueller, T.J., “Aerodynamic Characteristics of Low Aspect Ratio Wings at Low Reynolds Numbers,” Fixed and Flapping Wing Aerodynamics for Micro Air Vehicle Applications, Vol 195, Progress in Astronautics and Aeronautics, AIAA, 2001.

[20] Grasmeyer, J.M. and Keennon, M.T., “Development of the Black Widow Micro Air Vehicle,” Fixed and Flapping Wing Aerodynamics for Micro Air Vehicle Applications, Vol 195, Progress in Astronautics and Aeronautics, AIAA, 2001.

[21] Aerovironment, Inc., http://www.aerovironment.com/, Morovia, CA.

[22] Abdulrahim, M., Boothe, K., Lind, R. and Ifju, P., "Flight Characterization of Micro Air Vehicles using Morphing for Agility and Maneuvering," *SAE 2004 Transactions : Journal of Aerospace*, Vol. 113, No. 1, 2005, pp. 1704-1712.

---

[23] Abdulrahim, M., Garcia, H. and Lind, R., "Flight Characteristics of Shaping the Membrane Wing of a Micro Air Vehicle," *Journal of Aircraft*, Vol. 41, No. 1, January-February 2005, pp. 131-137.

[24] MLB Company, http://www.spyplanes.com/trochoid.html, Mountain View, CA.

[25] Albertani, R., Stanford, B., Hubner, J., and Ifju, P., "Characterization of Flexible-Wing MAVs: Aeroelastic and Propulsion Effects on Flying Qualities," *AIAA Atmospheric Flight Mechanics Conference and Exhibit*, San Francisco, CA, August 2005.

[26] University of Arizona Micro Air Vehicle Club, http://clubs.engr.arizona.edu/mav/, Location: Tucson, AZ.

[27] Null, W., and Shkarayev, S., "Effect of Camber on the Aerodynamics of Adaptive Wing Micro Air Vehicles," *2nd AIAA Flow Control Conference*, Portland, OR, July 2004.

[28] Pereira, J., and Chopra, I., "An Investigation of the Effects of Shroud Design Variables on the Hover Performance of a Shrouded-Rotor Micro Air Vehicle," *American Helicopter Society International Specialists' Meeting on Unmanned Rotorcraft Proceedings,* January, 2005.

[29] Parsons, E., Sirohi, J., and Chopra, I., "Micro Air Vehicle; Cycloidal Rotor Concept," *American Helicopter Society International Specialists' Meeting on Unmanned Rotorcraft Proceedings,* January, 2005.

---

[30] Kroo, I., and Kunz, P. “Mesoscale Flight and Miniature Rotorcraft Development,” Fixed and Flapping Wing Aerodynamics for Micro Air Vehicle Applications, Vol 195, Progress in Astronautics and Aeronautics, AIAA, 2001.

[31] “The Mesicopter: A Meso-scale Flight Vehicle,” http://www-aa.stanford.edu/mesicopter/, Stanford, CA.

[32] Sirohi, J., Tishchenko, M. and Chopra, I., “Design and Testing of a Micro-Aerial Vehicle with a Single Rotor and Turning Vanes,” *Proceedings of 61st Annual Forum of the American Helicopter Society*, Grapevine, TX, June 2004.

[33] Bohorquez, F., Samuel, P., Sirohi, J., Rudd, L., Pines, D. and Perel, R., “Design and Analysis and Performance of a Rotary Wing MAV,” *Journal of the American Helicopter Society*, Vol. 48, No. 2, pp. 80-90, April, 2003.

[34] Bohorquez, F., and Pines, D., “Rotor and Airfoil Design for Efficient Rotary Wing Micro Air Vehicles,” *Proceedings of the 61st Annual Forum of the American Helicopter Society,* Grapevine, TX, June 2004.

[35] Jones, K.D., Lund, T.C., and Platzer, M.F., “Experimental and Computational Investigation of Flapping Wing Propulsion for Micro Air Vehicles,” Fixed and Flapping Wing Aerodynamics for Micro Air Vehicle Applications, Vol 195, Progress in Astronautics and Aeronautics, AIAA, 2001.

[36] Jones, K.D., Bradshaw, C.J., Papadopoulos, J., and Platzer, M.F., “Development and Flight Testing of Flapping-Wing Propelled Micro Air Vehicles,” *2nd AIAA Unmanned*

Unlimited Systems, Technologies, and Operations (Aerospace, Land, and Sea) Conference and Workshop, San Diego, California, September 15-18, 2003, AIAA 2003-6549.

[37] Jones, K., Bradshaw, C., and Papadopoulos, J., "Improved Performance and Control of Flapping-Wing Propelled Micro Air Vehicles," *42nd AIAA Aerospace Sciences Meeting and Exhibit*, Reno, NV, January 2004.

[38] Rajagopalan, S., "Researchers Ape Nature with Flapping Wing Aircraft," The Washington Post, 1 Sept 2003.

[39] Frampton, K.D., Goldfarb, M., Monopoli, D., and Cveticanin, D., "Passive Aeroelastic Tailoring for Optimal Flapping Wings," Fixed and Flapping Wing Aerodynamics for Micro Air Vehicle Applications, Vol 195, Progress in Astronautics and Aeronautics, AIAA, 2001.

[40] Schenato, L., Deng, X., and Sastry, S., "Flight Control System for a Micromechanical Flying Insect: Architecture and Implementation," *Proceedings of the IEEE International Conference on Robotics and Automation*, Vol 2, 2001.

[41] Singh, B., Ramasamy, M., Chopra, I., and Leishman, G., "Experimental Studies on Insect-Based Flapping Wings for Micro Hovering Air Vehicles," *46th AIAA/ASME/ASCE/AHS/ASC Structures, Structural Dynamics, & Materials Conference*, Austin, TX, April 2005.

[42] Tarascio, M., and Chopra, I., “Design and Development of a Thrust Augmented Entomopter: An Advanced Flapping Wing Micro Hovering Air Vehicle,” *59th American Helicopter Society Forum*, Phoenix, AZ, May 2003.

[43] Bridges, A., “Flying Robots Create a Buzz,” Monterey County Herald, July 28, 2002.

[44] DeLaurier, J.D., “An Aerodynamic Model for Flapping-Wing Flight,” *Aeronautical Journal*, Vol. 97, April 1993, pages 125-130.

[45] Project Ornithopter, http://www.ornithopter.net/history_e.html, Toronto, Canada.

[46] Mueller, T., and DeLaurier, J., “Aerodynamics of Small Vehicles,” *Annual Review of Fluid Mechanics*, Vol 35, 2003.

[47] Pornsin-sirirak, T.N., Lee, S.W., Nassef, H., Grasmeyer, J., Tai, Y.C., Ho, C.M., and Keennon, M., “Titanium-Alloy MEMS Wing Technology for a Battery-Powered Ornithopter,” *The 13th IEEE Annual International Conference on MEMS*, Miyazaki, Japan, January 23-27, 2000, pp. 709-804.

[48] Keennon, M.T. and Grasmeyer, J.M., “Development of the Black Widow and Microbat MAVs and a Vision of the Future of MAV Design,” *AIAA/ICAS International Air and Space Symposium and Exposition*, AIAA 2003-2901.

[49] DelFly, http://www.delfly.nl, Location: Delft, The Netherlands.

---

[50] Malolan, V., Dineshkumar, M., and Baskar, V., “Design and Development of Flapping Wing Micro Air Vehicle,” *42nd AIAA Aerospace Sciences Meeting and Exhibit*, Reno, NV, January 2004.

[51] Muniappan, A., Baskar, V., and Duriyanandhand, V., “Lift and Thrust Characteristics of Flapping Wing Micro Air Vehicle,” *43rd AIAA Aerospace Sciences Meeting and Exhibit*, Reno, NV, January 2005.

[52] Ho, S., Nassef, H., Pornsinsirirak, N., Tai, Y., and Ho, C., “Unsteady Aerodynamics and Flow Control for Flapping Wing Flyers,” *Progress in Aerospace Sciences*, Vol 39, 2003.

[53] Vogel, S., Life in Moving Fluids, Princeton University Press, Princeton, NJ, 1994.

[54] Goldstein, S., Modern Developments in Fluid Dynamics, 1938, Reprint, Dover Publications, New York, 1965.

[55] Schmitz, F.W., Aerodynamik des Flugmodells, Carl Lange, Duisberg, Germany, 1960.

[56] Chronister, N., The Ornithopter Design Manual, 4th ed, The Ornithopter Society, 1999.

[57] Weis-Fogh, T. and Jensen, M., “Biology and Physics of Locust Flight,” *Philosophical Transactions of the Royal Society of London, B, 239.*

[58] Norberg, U.M., Vertebrate Flight, Springer-Verlag, Berlin, 1990, pp. 166-179.

---

[59] Sky Hooks and Rigging, “Coreless and Cored Motors,” http://www.skyhooks.ca/WMotcor.htm, Location: ON, Canada.

[60] Hobby People, “Cirrus Micro Joule Flight Pack,” http://www.hobbypeople.net/gallery/443413.asp, Location: Fountain Valley, CA.

[61] Hitec RCD USA, http://www.hitecrcd.com/, Location: Poway, CA.

[62] Dynamics Unlimited, http://www.slowfly.com/index.chtml, Location: Largo, FL.

[63] Plantraco Hobbies, http://www.plantraco.com/hobbies/, Location: SK, Canada.

[64] FlapDesign Software, http://www.ornithopter.org/flapdesign1.shtml, Location: Rochester, NY.

[65] Wiggins, L., “Structural Design and Analysis of a Kinematic Mechanism for a Morphing Hyper-Elliptic Cambered Span (HECS) Wing,” M.S. Thesis, Virginia Tech, 2003.